Article

High-Latitude Depositional Systems, Provenance, and Basinal Setting of the Late Cretaceous Cantwell Basin, Denali National Park and Preserve, Alaska: A Stratigraphic Framework for Paleontological and Paleoclimatic Studies

Brandon Keough * and **Kenneth Ridgway**

Department of Earth, Atmospheric, and Planetary Sciences, Purdue University, West Lafayette, IN 47907, USA
* Correspondence: brandonkeough14@gmail.com

Abstract: The Cantwell Formation of the central Alaska Range provides a robust archive of high-latitude, Late Cretaceous depositional systems and paleo-floral/faunal assemblages. Our stratigraphic analysis defines two mappable members. The lower member (1500–2000 m thick) represents vegetated alluvial fan and braided fluvial systems that transition up-section to fluvial–estuarine systems that drained into an inland continental seaway. The upper member (~2000 m thick) represents estuarine–marginal marine and lacustrine systems. Previous paleontological studies demonstrate that the Cantwell basin was populated by various dinosaurs, fishes, bivalves, birds, and marginal marine micro-organisms. Integration of new and published geologic mapping allows for reconstruction of depositional systems at the basin scale and provides additional paleogeographic context. The northern basin margin was defined by a previously unrecognized south-verging thrust belt, whereas the southern margin of the basin was defined by a north-verging thrust belt inboard of an active magmatic arc. Sediment sources interpreted from U-Pb detrital zircon geochronology included the coeval magmatic arc and older Cretaceous plutons, and Proterozoic–Mesozoic strata exhumed along the basin margins. Results of our study provide a depositional, stratigraphic, and structural framework that may serve as a guide for future paleontological and paleoclimatic investigations of Late Cretaceous Arctic environments of the Cantwell basin.

Keywords: basin analysis; Cantwell basin; Late Cretaceous; tectonics; paleoclimate; paleontology

1. Introduction

The Cantwell basin, located in the central Alaska Range, contains a rich archive of Late Cretaceous high-latitude depositional systems, paleobiological ecosystems, and tectonics of the northwestern Cordillera of North America. The basin consists of 4 km of siliciclastic strata, the Cantwell Formation, exposed between the Hines Creek and Denali fault systems (Figures 1 and 2) [1,2]. The Cantwell Formation is characterized by thick successions of conglomerate, sandstone, mudstone, and minor coal and limestone interpreted to represent alluvial fan, braided stream, lacustrine, and marginal marine environments [2,3]. Since the initial geologic mapping and sedimentary studies of the Cantwell Formation, abundant trace fossils of theropods, ceratopsians, hadrosaurs, therizinosaurs, fishes, and pterosaurs have been documented, along with high-latitude paleoclimate records e.g., Refs. [4–9]. The Cantwell Formation also contains a record of the syndepositional and post-depositional deformational processes that constructed the alpine topography of the central Alaska Range [1,2,10,11]. Despite the importance of the Cantwell basin from a stratigraphic, paleobiologic, and regional tectonic perspective, an integrated stratigraphic and structural framework has not been fully developed.

The primary goal of our study is to establish a detailed stratigraphic framework for the Cantwell basin, integrating new and previously published geologic mapping data to

reconstruct depositional systems at a basin scale from deformed strata of the Cantwell Formation. Additionally, we use modern techniques for provenance analysis to develop a more regional perspective on the paleogeographic and tectonic context of the Cantwell basin. With these goals in mind, we present the following components of our analysis: (1) a composite representative section that we correlate throughout the basin; (2) an updated geologic map compilation and three structural cross-sections within the most accessible and continuous exposures of the Cantwell Formation in Denali National Park and Preserve (i.e., the western part of the basin); (3) U-Pb detrital zircon ages (N = 13; n = 4657) with stratigraphic control to add a new perspective to a previous composition-based provenance analysis [2]; and (4) an integrated interpretation of the basin configuration and regional paleogeographic setting of the Cantwell basin.

The results of our study provide an updated basin framework relevant to future studies of Late Cretaceous paleontology, paleoclimate, and tectonics in the northern North American Cordillera. Reconstruction of paleo-environments associated with vertebrate fossil-bearing assemblages has the potential to reveal how high-latitude Cretaceous depositional systems and their related ecosystems responded to changing climate conditions e.g., Ref. [7]. Changes in climate are known to have particularly profound impacts in Arctic environments and these changes are often best preserved in the sedimentary record e.g., Refs. [12,13]. Our analysis, hopefully, will also provide additional geologic content for the over 500,000 annual visitors to Denali National Park and Preserve that view and interact with this scenic landscape.

2. Geologic Background

2.1. Paleontology and Paleoclimate

Ongoing interest in the Cantwell Formation has stemmed from recent discoveries of abundant bird and dinosaur trackways, including theropods, ceratopsians, pterosaurs, therizinosaurs, and hadrosaurs e.g., Refs. [4,6,14–18]. Various bird trackways, fishes, and crayfish burrows have also been documented [4,5]. The most prolific dinosaur and bird tracksites are associated with fluvial and overbank deposits, primarily in the middle-upper part of the Cantwell Formation e.g., Ref. [6]. These strata are also rich in leaf fossils, wood fragments, and other organic matter. Stable isotopes from these materials have been used to determine annual temperature ranges and serve as a proxy for paleo-precipitation rates. These data yield a mean annual temperature of 7.4 ± 2.4 °C, with an annual temperature range from −2.3 ± 3.8 °C to 17.1 ± 3.2 °C (mean temperatures for the coldest and warmest months, respectively) [9].

Along with the Cantwell basin, vertebrate fossil assemblages, including several dinosaur species, have been reported in Mid-Upper Cretaceous strata throughout Alaska. In southern Alaska, dinosaur trackways have been identified in forearc basin strata of the Matanuska basin [19] and the Chignik Formation of the Alaska Peninsula [20]. Trackways of theropods and ornithopods have been identified in proximal foreland basin strata of the Beaver Lake formation in the Nutzotin Mountains of Wrangell–St. Elias National Park and Preserve (Figure 1) [21]. In interior Alaska, one dinosaur track has been identified in fluvial strata exposed in the Charley River thrust belt within Yukon–Charley Rivers National Preserve [22]. Finally, the Prince Creek Formation exposed on the North Slope of Alaska has yielded a rich assemblage of dinosaur and bird trackways e.g., Refs. [23–25].
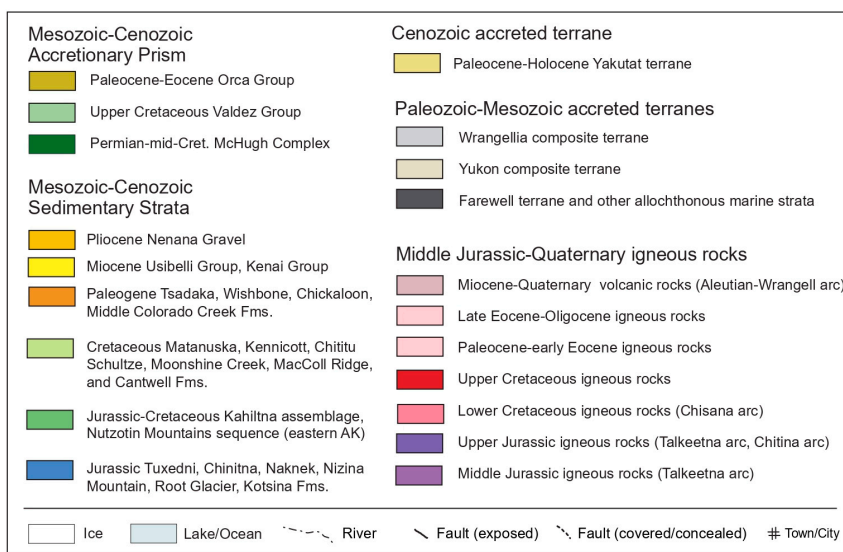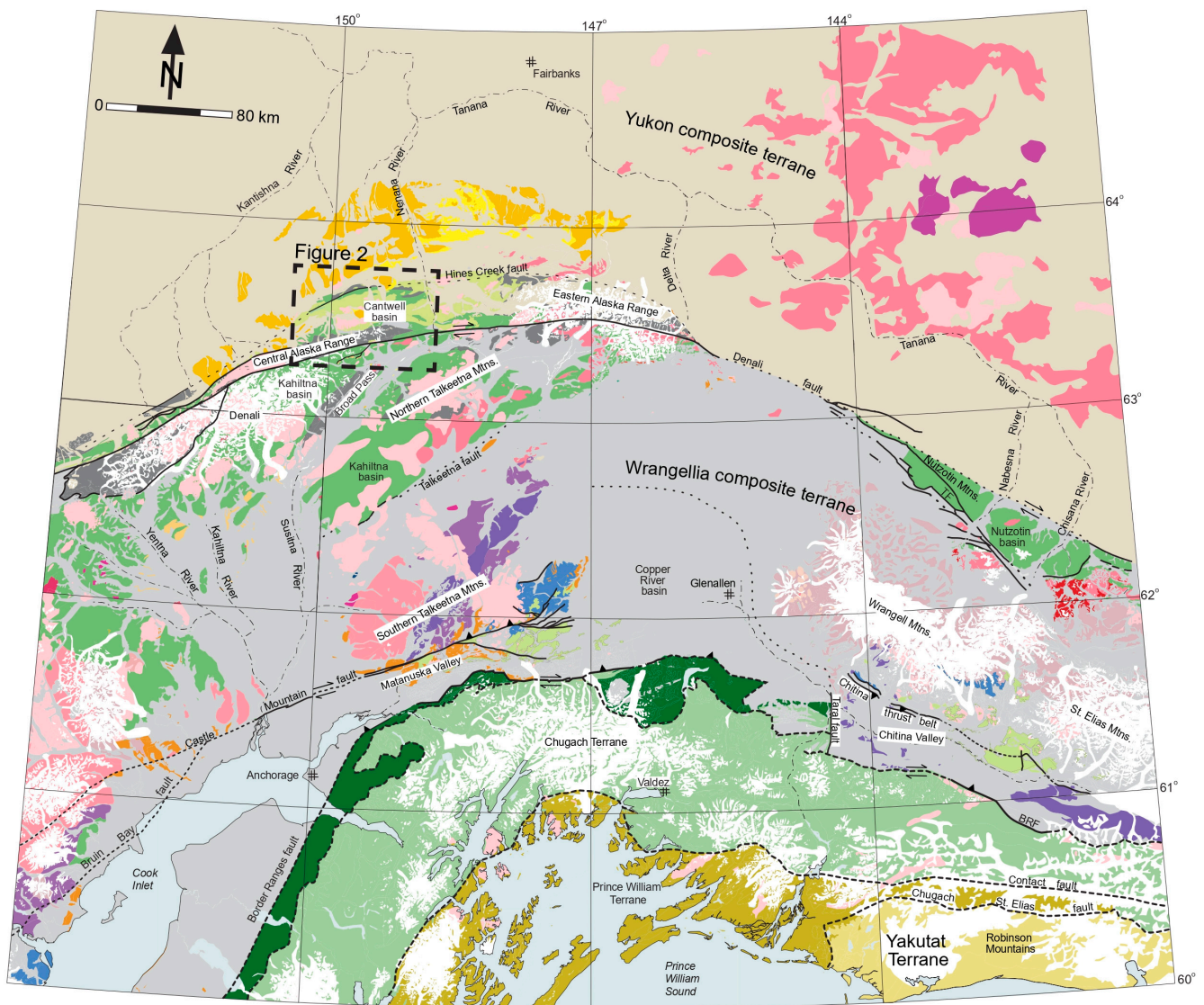
Figure 1. Generalized geologic map of south-central Alaska, modified from Trop and Ridgway (2007). Box labeled Figure 2 shows the location of the study area; this area is enlarged in Figure 2.

Workers have also begun to use various proxies archived in the sedimentary record to search for regional links between high-latitude, Late Cretaceous Arctic tracksites and broader climate patterns e.g., Refs. [7,26]. In addition to the Cantwell Formation, terrestrial assemblages that have been the focus of detailed sedimentological and paleoclimate studies include the Prince Creek Formation (North Slope of Alaska) and the Chignik Formation (southern Alaska) e.g., Refs. [5,7–9,27]. Results of these studies suggest that differences in climate over ~20° of paleo-latitude likely served as a key driver of differences observed in large-bodied herbivore populations [7]. Initial studies of paleoclimate have also begun to demonstrate links to more global climate patterns during the late Campanian-early Maastrichtian. For example, δ^{13}C isotope analysis of organic material suggests that a mid-Maastrichtian warming event recognized globally is also recorded in the Cantwell Formation [8].

2.2. Existing Structural and Stratigraphic Framework

2.2.1. Age Control

The age of the Cantwell Formation was originally determined using plant fossils, which resulted in conflicting age determinations ranging from Cretaceous to Paleocene [28–31]. For several decades, the accepted age for the Cantwell Formation was Paleocene based on paleobotanical data [30]. More refined age constraints now include palynological data with stratigraphic control [2] and 14 bentonites dated using U-Pb Laser Ablation Inductively Coupled Plasma Mass Spectrometry (LA-ICP-MS) [3,8,11,18]. Ridgway et al. [2] reported results of palynologic analyses from 135 mudstone samples that yielded an age range of late Campanian–early Maastrichtian for the Cantwell Formation. Recently dated bentonites yielded ages between 88.0 ± 0.4 Ma and 67.8 ± 0.2 Ma [3,8,11,18]. Seven locations for which published bentonites are reported are within our general study area, though localities with bentonite ages remain difficult to correlate with measured stratigraphic sections from both this study and previously published studies due to the structural complexity e.g., Ref. [11].

2.2.2. Previous Stratigraphic Analyses of the Cantwell Basin

Initial geologic mapping and stratigraphic studies of the Cantwell basin were part of regional analyses primarily focused on the area east of the Nenana River (Figure 2) [1,31,32]. The first workers to classify the Cantwell basin interpreted the basin as a Paleogene, strike-slip pull-apart basin related to the Hines Creek and Denali fault systems e.g., Ref. [1]. Ridgway et al. [2] later re-interpreted the Cantwell basin as a Late Cretaceous thrust-top basin related to the final stages of Mesozoic collisional tectonics. The reconstruction of depositional environments from isolated exposures both east and west of the Nenana River led to the development of a basin model by Ridgway et al. [2], in which alluvial fan systems merged into axial braided fluvial systems that drained the basin to the east. Extensive lacustrine deposits were thought to be most prevalent along the southern basin margin, consistent with an asymmetric, southward-dipping basin floor. Marginal marine influence near the top of the Cantwell Formation is suggested by the presence of marginal marine dinoflagellates, and oncolitic and algal-laminated limestone beds at Double Mountain (DM1 in Figure 2) [2]. It is important to note that these early studies included limited data from exposures of the Cantwell Formation located east of the Nenana River (Figure 2). The exposures in that region are included in regional mapping studies [33,34], but have not been integrated into detailed stratigraphic analyses of the Cantwell basin, including this study. Finally, the most recent stratigraphic studies have focused on the Tattler Creek/Sable Mountain area (Figure 2), where robust paleobotanical and paleontological datasets have been collected with stratigraphic control and integrated with interpretations of alluvial–fluvial depositional environments e.g., Refs. [6,9].
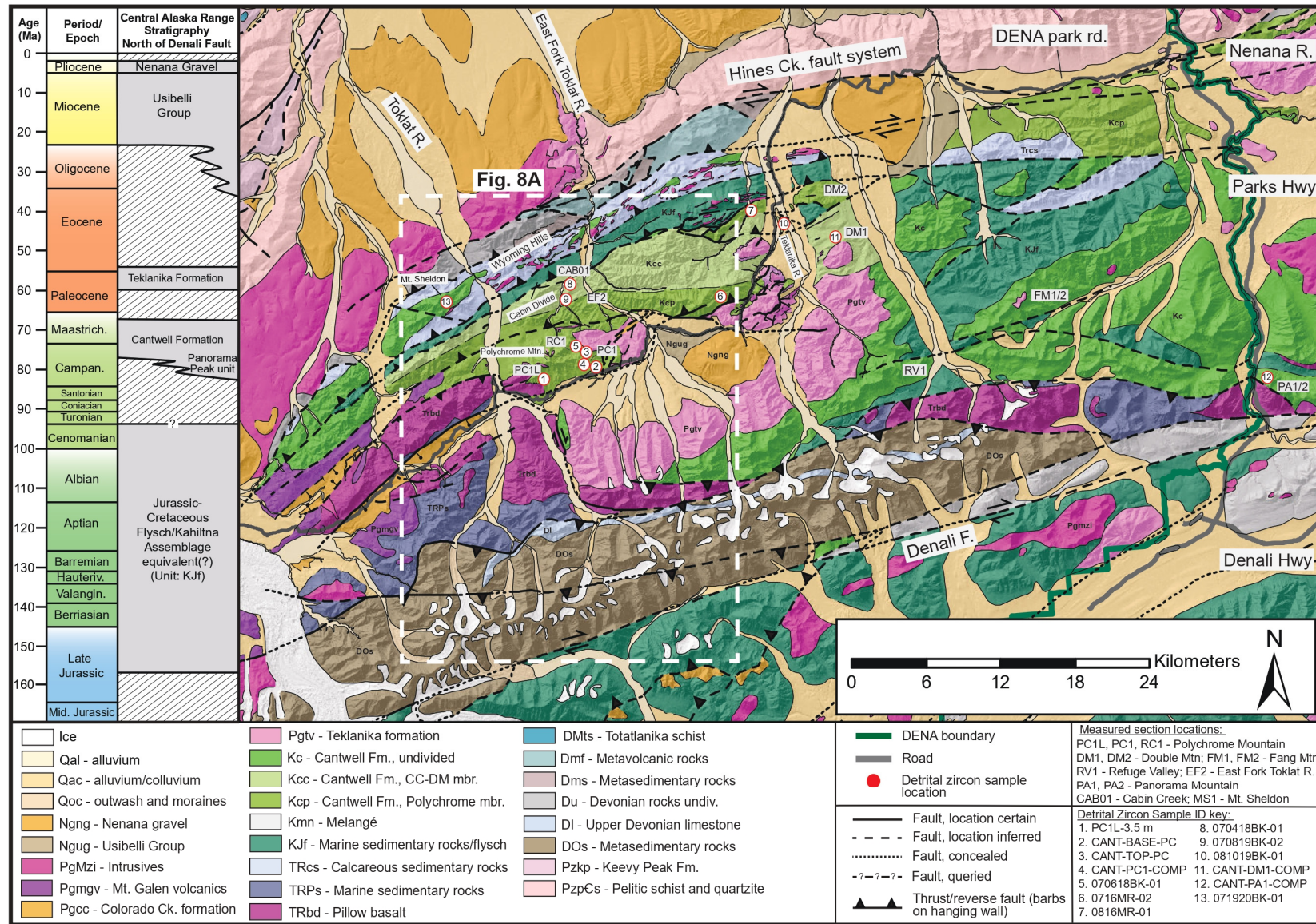
Figure 2. Geologic map of the study area in the northeastern corner of Denali National Park and Preserve. The stratigraphic chart shows the Middle-Jurassic–Cenozoic stratigraphy of the study area (modified from Trop et al. [11]). The areal extent of this map is shown by the dashed box in Figure 1. The locations of measured sections referenced in Figures 3 and 6 are labelled using the abbreviations shown in the key. Geologic mapping data are a compilation of new data described in the text and the data of Reed [35], Gilbert and Redman [36], Csejtey et al. [33,34], and Cole et al. [10]. The Cantwell Formation is subdivided into the Polychrome member (Kcp—lower member) and the Cabin Creek–Double Mountain member (Kcc—upper member).

2.2.3. Tectonic Setting of the Central Alaska Range

　　The Cantwell basin formed in a region of polyphase deformation dominated by collisional tectonics from the Late Jurassic through the Cretaceous. This region has been termed the Alaska Range Suture Zone (ARSZ), with the present-day surface expression defined as the region between the Talkeetna fault to the south and the Hines Creek fault to the north (Figure 1) e.g., Refs. [11,37–41]. The ARSZ has been studied extensively and is divided into three components: (1) the ancestral North American margin to the north, which served as the Mesozoic collisional backstop (Yukon composite terrane in Figure 1); (2) the oceanic Wrangellia composite terrane (WCT) to the south (Figure 1), which is thought to have collided obliquely from south to north along the continental margin [38,42,43]; and (3) deformed and metamorphosed sedimentary basin assemblages that represent the Jurassic–Cretaceous ocean basin between the ancestral North American margin and the WCT that was subsequently segmented and eventually fully closed in the collisional zone (e.g., Kahiltna basin) [43,44]. The part of the Cantwell basin exposed in our study area also overlaps a slightly older, Late Jurassic–Early Cretaceous accretionary zone associated with the interpreted collision of the allochthonous Farewell terrane with the ancestral North American margin [45]. Much of the Cantwell Formation in our study area was deposited unconformably atop Upper Triassic basalt interpreted as part of the Farewell terrane (unit TRbd in Figure 2) e.g., Refs. [35,36,45], whereas along the northern basin margin, the Cantwell Formation overlies deformed Mesozoic marine strata interpreted to be associated with the ancestral North American margin (unit TRcs in Figure 2) [45].

3. Methods

3.1. Stratigraphic Nomenclature

　　Early studies of the Cantwell Formation typically used the terminology "upper" and "lower" Cantwell Formation to refer to the Upper Paleocene–Lower Eocene Teklanika volcanic strata and the Upper Cretaceous siliciclastic Cantwell Formation, respectively e.g., Refs. [2,30,34]. More recently, the long-standing name Teklanika Formation [46] has been used for the volcanic sequence, while "Cantwell Formation" refers only to the sedimentary strata e.g., Ref. [11]. We conform to this terminology as separate formations are warranted by distinct lithologies, a depositional hiatus, and an angular unconformity between the Cantwell Formation and the Teklanika Formation volcanic strata in some parts of the basin. For the purposes of our stratigraphic analysis, we further divide the Cantwell Formation into two informal members. We use the term Polychrome member to refer to a lower member and the term Cabin Creek–Double Mountain member to refer to an upper member. The sedimentological basis for these members is described in the Results section.

3.2. Stratigraphic Analysis

　　Our stratigraphic analysis was based on the construction of a composite representative section for the Cantwell Formation (Figure 3). We identified several exposures between the Toklat River and the East Fork of the Toklat River that comprise common lithofacies of the Cantwell Formation (Figure 2). Due to the structural complexity of the basin, this composite representative section does not perfectly record the stratigraphic thickness of the Cantwell Formation. We accounted for these challenges by completing our own mapping in select parts of the study area to develop as complete a stratigraphic framework as possible,

particularly where measured sections were separated by faults. Stratigraphic data were collected using the standard methods of measuring a section with a Jacob's staff. Data collected from stratigraphic sections included bedding thickness, bedding geometry, grain size, sedimentary structures, color, compositional clast counts of conglomerate, maximum particle size measurements, and the documentation of fossils. The latitude and longitude of the base and top of measured sections that comprised our composite representative section are available in Supplementary File S1.
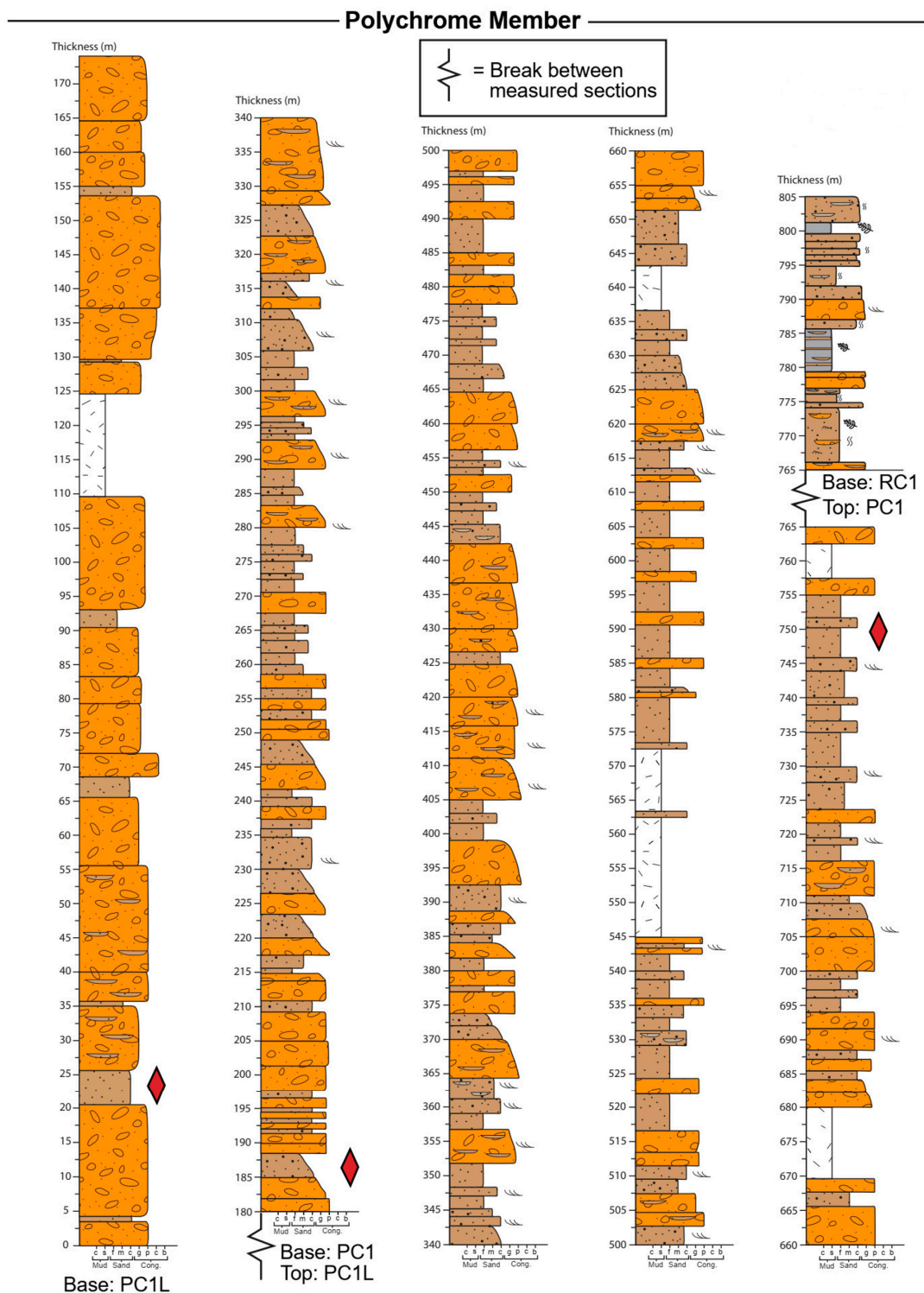
Figure 3. *Cont.*
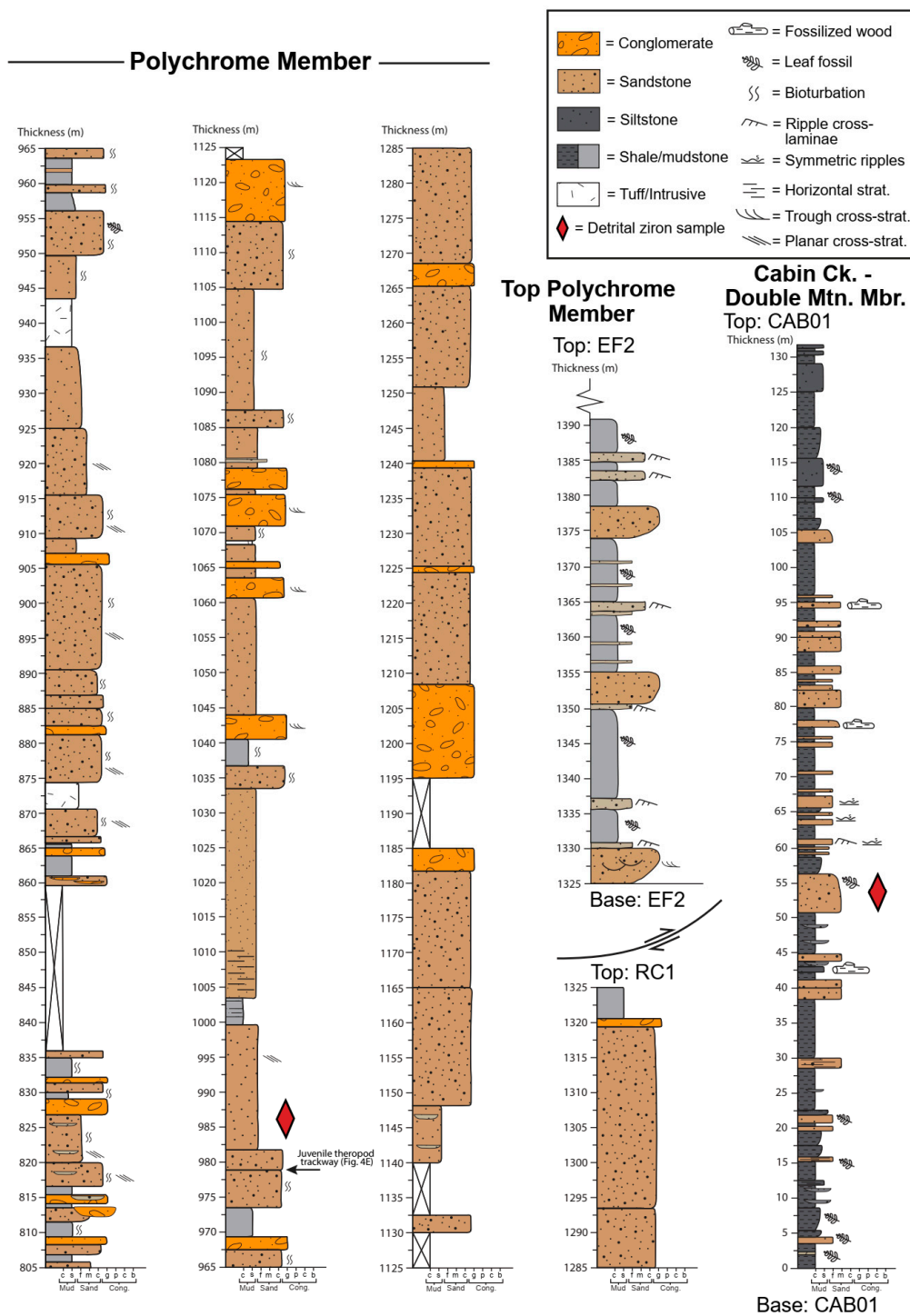
Figure 3. Composite representative stratigraphic section of the Cantwell Formation. Note that section PC1 on the eastern flank of Polychrome Mountain is reported by Trop [47]; all other sections were measured as part of this study. Locations indicated by measured section abbreviations are as follows (also labelled on Figure 2): PC1L—Polychrome Mountain, south side; PC1—Polychrome Mountain, southeast flank; RC1—Polychrome Mountain, northeast flank; EF2—East Fork of the Toklat River, west bank; CAB01—Cabin Divide.

3.3. Geologic Mapping

Geologic mapping was conducted over two field seasons as part of a USGS EDMAP cooperative project. The bulk of our mapping was conducted along the Toklat River corridor and in the region between the Toklat River and the East Fork of the Toklat River north of the Denali Park Road (Figure 2). In this paper, we present results of our mapping compiled with published mapping data of Reed [35], Gilbert and Redman [36], Csejtey et al. [34], and Cole et al. [10], and previously compiled data of Wilson et al. [48]. The data compilation was completed using ESRI ArcMap version 10.6.2. Our compilation also merged multiple generations of mapping along the Healy/Mt. McKinley quadrangle boundary, which lies just east of the Toklat River.

3.4. U-Pb Detrital Zircon Geochronology

All detrital zircon samples were crushed, separated, and mounted at the Arizona LaserChron Center via standardized methods of physical and chemical separation [49–52]. SEM-generated cathodoluminescence (CL) images were used to select grains without complex crystallographic domains, and back-scattered electron (BSE) images were used to avoid grains that were not zircon. Grains were selected randomly without intentional bias toward size or shape, and fractures were avoided to minimize the introduction of common Pb. All U-Pb analyses were conducted using laser ablation inductively coupled mass spectrometry (LA-ICPMS). Some analyses were conducted using a Thermo Element2 single collector ICPMS and some samples were analyzed in 2019 and 2020 using a Nu Plasma multicollector ICPMS [51]. Analyses conducted on the Nu Plasma multicollector ICPMS utilized rapid acquisition (3s/analysis) protocols as outlined by Sundell et al. [53]. A spot diameter of 20–30 μm was used for all analyses. Data reduction for analyses conducted on the Element2 was completed using "AgeCalc" protocols; in-house protocols developed by the ALC. Data reduction for analyses conducted on the Nu Plasma Multicollector was completed using AgeCalcML [53]. Both reductions include a common Pb correction (cf. [54]). Probability density plots of detrital zircon data were generated using Isoplot 4.15 [55], and age peaks for detrital zircon spectra were calculated using Age Pick software [49]. Sample locations are available in Supplementary File S1, probability density plots by sample are available in Supplementary File S2, and U-Pb data are available in Supplementary File S3.

Analysis of detrital zircon data in our study was utilized primarily for provenance interpretations. We do not report maximum depositional ages for our detrital zircon geochronology dataset since, as has been recognized by previous workers, Pb loss is likely prevalent in zircons from the Cantwell Formation [11]. Anomalously young ages that comprise young age tails are present in published U-Pb zircon data from the Cantwell basin [11], as well as our detrital zircon data. Given that these anomalously young ages consistently fall within the time interval of peak magmatism associated with the Teklanika Formation at ~57 Ma [10], it is likely that leaching of Pb occurred in the presence of hydrothermal fluids at this time [56].

4. Stratigraphic Framework

We divide the Cantwell Formation into two informal stratigraphic members: a lower member defined as the Polychrome member, and an upper member defined as the Cabin Creek–Double Mountain member. Figure 3 shows detailed sedimentological data for our composite representative section; Figures 4 and 5 illustrate the distinctive sedimentological features of each member; and Figure 6 shows lithostratigraphic correlations by member between measured sections that comprise our composite section and other published measured sections.
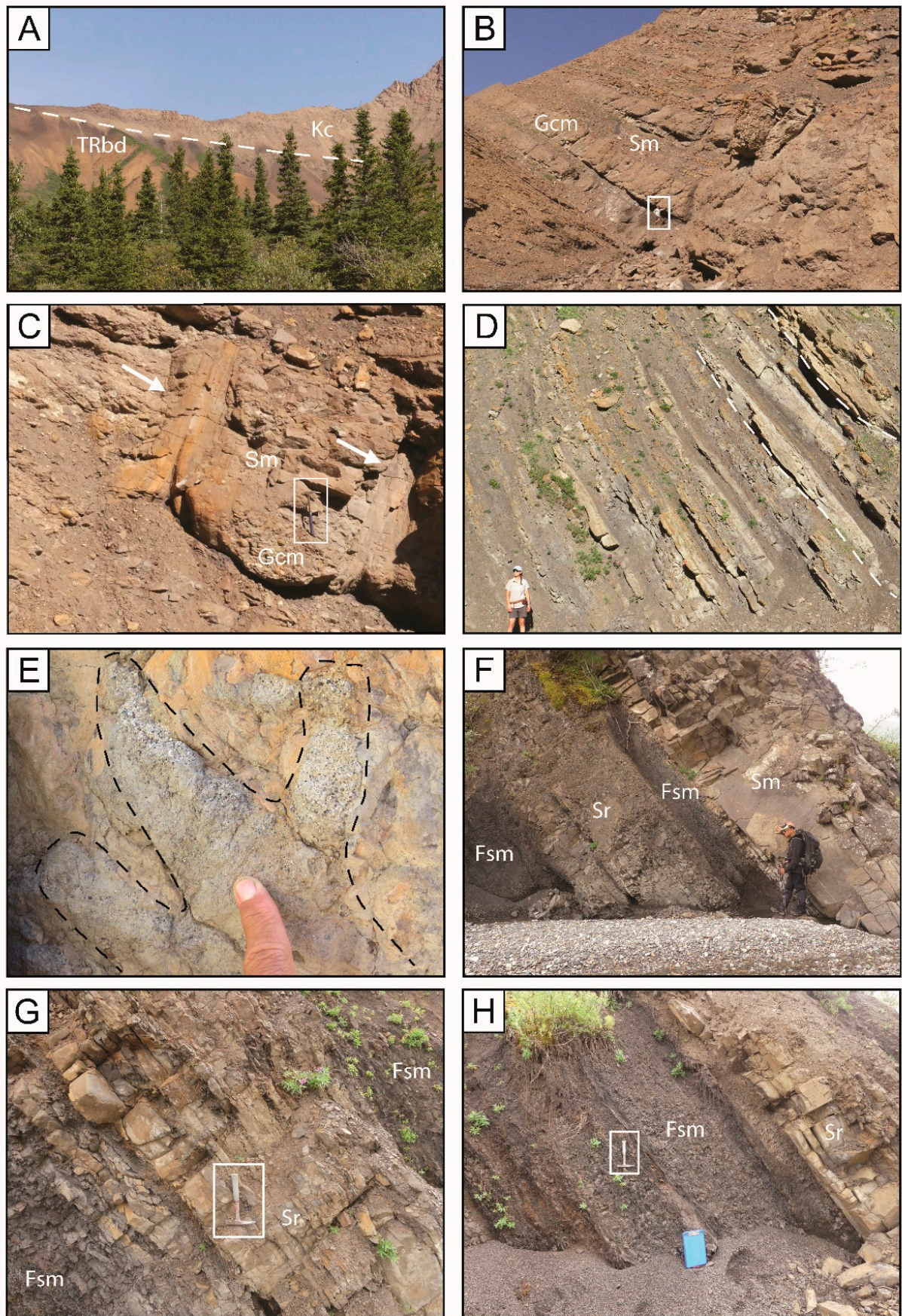
Figure 4. Field photographs of the Polychrome member in stratigraphic order. (**A**) Photo showing the depositional contact (dashed white line) between the base of the Polychrome member (Kc) and

Upper Triassic basalt (TRbd). The base of section PC1L is located at this contact on the south flank of Polychrome Mountain. View is towards the west–northwest. (**B**) Interbedded sheet conglomerate (Gcm), coarse sandstone (Sm), and minor siltstone characteristic of the lower Polychrome member (PC1). A person wearing a white shirt for scale in the white box. (**C**) In situ tree fossils preserved in the lower Polychrome member (white arrows). Pebble–cobble conglomerate is concentrated around the base of the trees. Hammer for scale in the white box. (**D**) Interbedded sandstone, siltstone, and channelized granule conglomerate characteristic of the middle Polychrome member (RC1). The dashed white lines follow the base of lenticular sandstone beds interpreted as shallow channel bodies. A person for scale in the lower left corner. Beds dip to the right. (**E**) Juvenile theropod trackway (outlined by the black dashed line) on the base of a coarse-grained sandstone bed in the same stratigraphic section depicted in (**D**). Finger for scale. (**F**) Interbedded carbonaceous mudstone (Fsm); thin-bedded, fine-grained ripple cross-stratified sandstone (Sr); and medium-grained, massive and trough cross-stratified sandstone (Sm). This combination of lithofacies is characteristic of the more mud-rich upper Polychrome member (EF2). Note sharp contacts between lithofacies. A person for scale. Bedding dips to the right. (**G**) Thin-bedded, ripple cross-stratified, fine-grained sandstone with mud drapes and organic-rich mats (Sr) surrounded by carbonaceous, nodular siltstone (Fsm) (EF2). Hammer for scale in the white box. Bedding dips to the right. (**H**) Carbonaceous siltstone with abundant organic matter (Fsm) and lignite abruptly overlain by ripple cross-stratified, tabular sandstone (Sr). Hammer for scale in the white box. Bedding dips to the right.
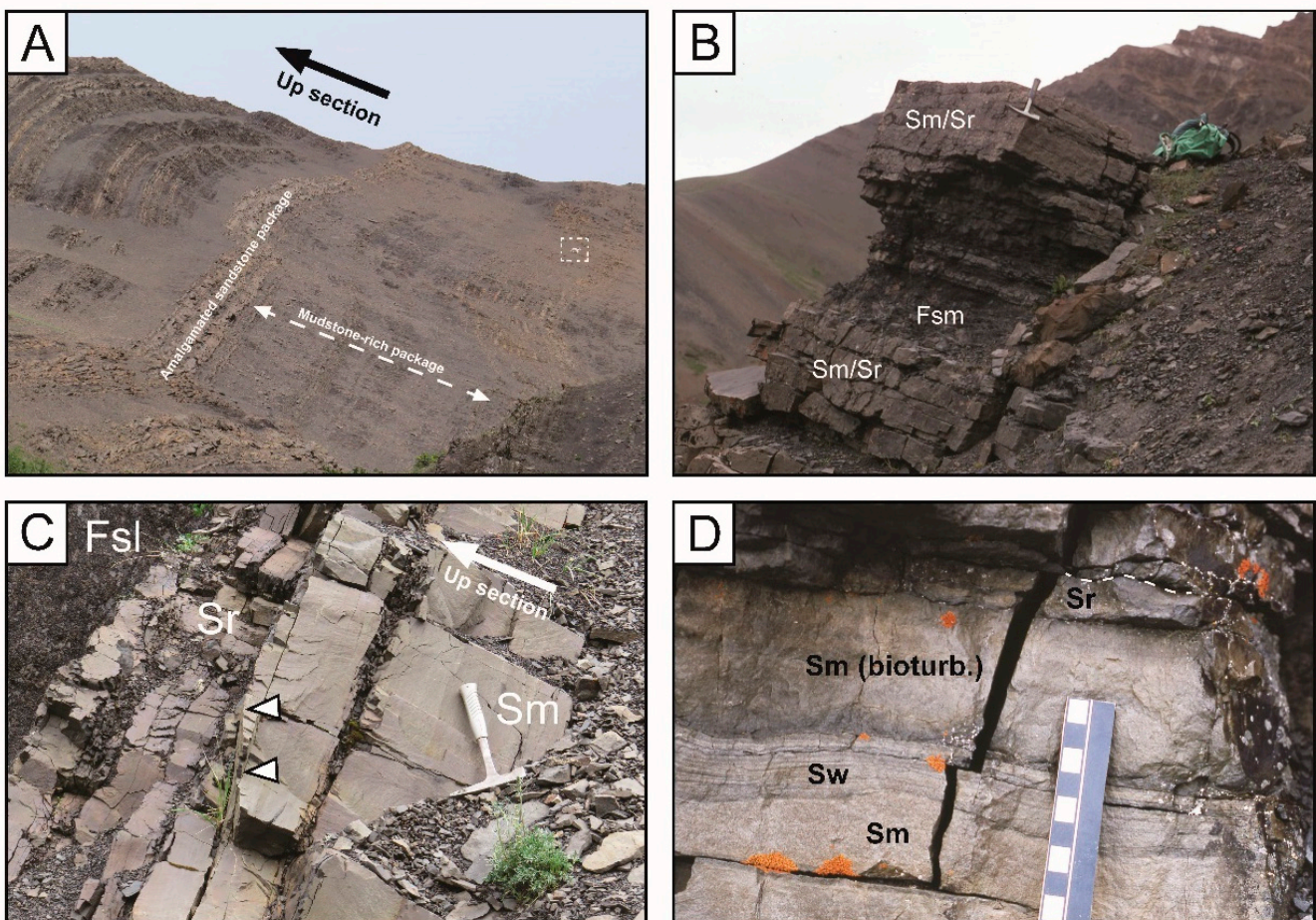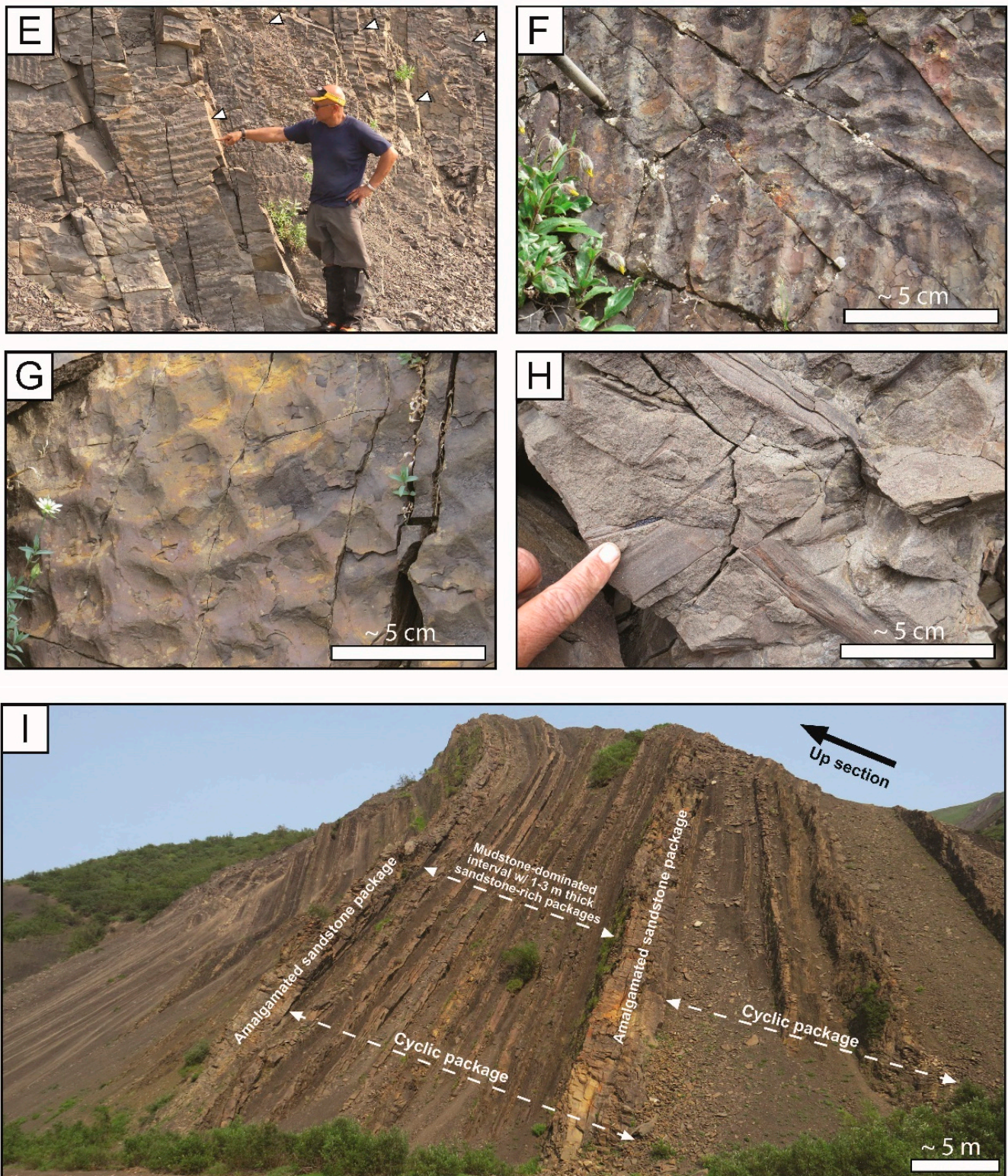

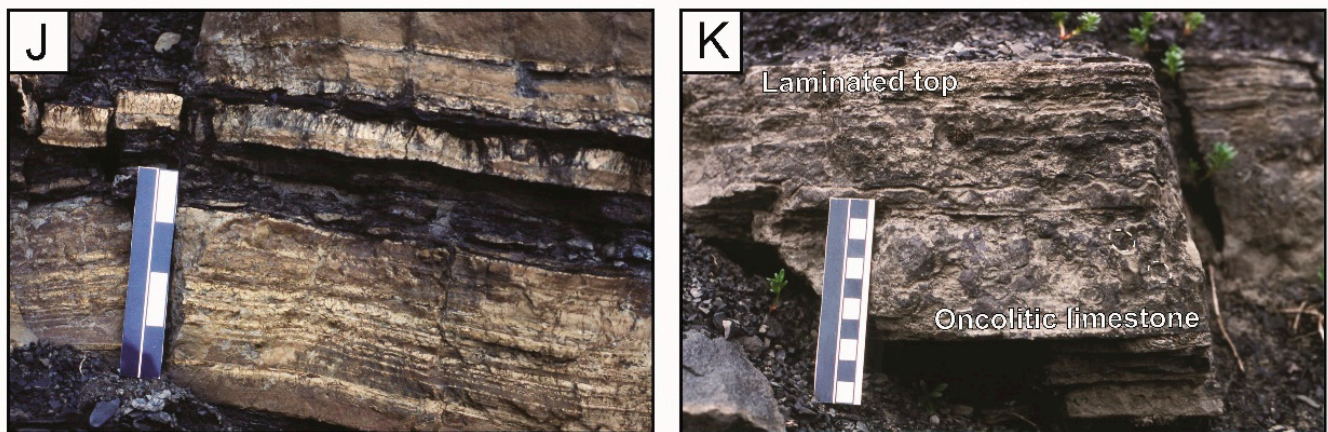**Figure 5.** *Cont.*

Figure 5. *Cont.*

Figure 5. Field photographs of the Cabin Creek–Double Mountain member. (**A**) Photograph of section CAB01 taken facing southeast. The exposure is dominated by thick mudstone intervals (dark beds) interbedded with 1–3 m thick sandstone packages. The most resistant beds in the exposure comprise 5–7 m thick amalgamated sandstone packages (yellow beds). Upright beds dip steeply to the left and are folded. Dall sheep for scale in the dashed white box. (**B**) Field photo of an amalgamated sandstone package exposed at Double Mountain. Massive and ripple cross-stratified sandstone beds (Sm/Sr) which are 10–30 cm thick comprise 75 to 100 cm thick units separated by massive mudstone (Fsm). Rock hammer and green backpack for scale. (**C**) Detailed photo of an approximately 1.5 m thick sandstone-dominated package. Internal bedding thickness thins upward with thin shale breaks between individual beds. A low-angle lateral accretion surface is indicated by the white triangles. Sandstone transitions from massive at the base (Sm) to ripple cross-stratified (Sr) at the top of the package. Fsl = laminated siltstone. Hammer for scale. (**D**) Detailed photograph of individual sandstone beds within a sandstone package at Double Mountain. The lower bed grades upward from fine-grained, massive sandstone at the base (Sm) to wavy-bedded sandstone at the top (Sw). Dark, mm scale units in Sw interval are mudstone drapes. The middle bed is bioturbated, massive sandstone capped by a thin, ripple cross-stratified (Sr) sandstone bed. An exposed cross-section of a symmetric ripple is highlighted by the dashed white line at the top of the bed. Divisions on the scale bar are 1 cm. (**E**) Symmetric ripples exposed on the tops of vertical sandstone beds at Cabin Creek. Note that the ripples are present on the top of every sandstone bed visible in the photograph, representing the ubiquitous nature of the symmetric ripples in sandstone packages. (**F**) Symmetric ripples on the top of a fine-grained sandstone bed at section CAB01. (**G**) Interference ripples on the top of a fine-grained sandstone bed (CAB01). (**H**) Casts and impressions of wood fragments concentrated at the base of a sandstone-rich package at Cabin Creek. The finger is pointing to a small coalified fragment (dark material). (**I**) Field photograph of section CAB01 taken facing southeast. Resistant sandstone-dominated intervals ~5–7 m thick bound a representative cyclic package containing a mudstone-dominated interval with interbedded 1–3 m thick sandstone-rich packages (lighter-colored beds). These beds are deformed in the footwall of the Cabin Divide fault. (**J**) Algal laminated limestone beds interbedded with marginal marine dinoflagellate-bearing shale at Double Mountain. Divisions on the scale bar are 2.5 cm. (**K**) Oncolitic limestone interbedded with marginal marine dinoflagellate-bearing shale at Double Mountain. Two of the oncolites are noted by dashed white ovals. The top of the oncolitic limestone bed transitions to algal laminated limestone. Divisions on the scale bar are 1 cm.

Figure 6. Stratigraphic cross-section correlating measured sections from this study with previously published measured sections (e.g., Ridgway et al. [2]; Trop [47]). The gradational contact between the Polychrome and Cabin Creek–Double Mountain members is used as a datum. The Cabin Divide fault (CDF) truncates stratigraphy along the northern basin margin and section MS1 is structurally isolated and in unconformable contact with underlying Upper Triassic submarine strata (TRcs).

4.1. Cantwell Formation Stratigraphy—Polychrome Member

4.1.1. Representative Locations and Measured Sections

The lower part of the Polychrome member is best exposed on the southern and eastern flanks of Polychrome Mountain, and the upper part is best exposed in the Tattler Creek/Sable Pass area and along the East Fork of the Toklat River (Figure 2). The Polychrome member is represented by our measured sections PC1L, RC1, and EF2, and also PC1 of Trop [47] (Figure 3). The base of section PC1L corresponds to an unconformable depositional contact between the Cantwell Formation and Upper Triassic basalt (TRbd in Figure 4A).

4.1.2. Sedimentology

The Polychrome member fines gradationally upward and is characterized in the lowermost 180 m (Section PC1L in Figure 3) by clast-supported, cobble–boulder conglomerate with a sandy matrix and interbedded massive, coarse-grained sandstone. Conglomerate clasts are well-rounded but poorly organized, lacking clear imbrication. Individual conglomerate beds are several meters thick, laterally continuous, and sometimes include localized lenses of coarse-grained sandstone. The average maximum particle size is 11.7 cm, though some clasts recorded are as large as 28 cm. Coarse–very-coarse-grained, massive sandstone intervals range in thickness from 1 to 4 m and comprise less than 10% of the total stratigraphic thickness in section PC1L (Figure 3).

The middle ~1200 m of the Polychrome member is characterized by interbedded pebble–cobble conglomerate, medium-grained sandstone, and minor siltstone (Figure 3). This part of the stratigraphy generally continues to fine upward, though some cyclicity exists between conglomerate-dominated and sandstone-dominated packages within a stratigraphic section of several hundred meters. In conglomerate-dominated successions such as in much of section PC1 (Figure 3), conglomerate beds range from one to several meters thick and are laterally continuous with tabular geometries (Figure 4B). Conglomerate beds are clast-supported and well organized, and clast imbrication is common. The average maximum particle size is 6 cm (Section PC1 of Trop, [47] and Ridgway et al. [2]). Sheet conglomerates are interbedded with lenses of medium-coarse-grained, trough cross-stratified sandstone, massive sandstone, and minor siltstone. Multiple upright tree casts were observed where pebble–cobble conglomerate is concentrated around the base of the fossilized trees, and interbedded pebble conglomerate, sandstone, and siltstone encases the upper part of the trunks (Figure 4C).

Sandstone-dominated intervals, best represented by our measured section RC1, are characterized by medium-coarse-grained sandstone beds with abundant internal scouring and planar and trough cross-stratification (Figure 3). Granule–pebble lags are common at the base of scour surfaces and transported fossilized plant fragments are abundant. Shallow, lenticular bodies fine upward from granule–pebble conglomerate at the base to massive, medium-grained sandstone at the top. The average maximum particle size of conglomerate beds is 3.5 cm, and the thickness of these bodies rarely exceeds three meters. Interbedded massive and ripple cross-stratified siltstone and fine-grained sandstone beds display abundant mottling and other pedogenic structures, and thin, organic-rich mudstone beds are sometimes present. Fossils most commonly include leaf imprints in fine-grained beds, though a relatively small, likely juvenile theropod trackway was found on the base of one coarse-grained sandstone bed (Figure 4E).

Measured section EF2, along the west bank of the East Fork of the Toklat River, documents lithofacies diagnostic of the uppermost Polychrome member (Figure 3). The

maximum thickness of this part of the stratigraphy is uncertain, but our observations at section EF2 and along Tattler Creek suggest that at least 450 m of similar strata are present. Section EF2 is characterized by three distinctive lithofacies separated by sharp contacts (Figure 4F–H): (1) Medium-coarse-grained, massive and trough cross-stratified sandstone with abundant internal scouring (Sm in Figure 4F). Sandstone is internally organized in broadly lenticular bodies several meters thick with individual bedding thicknesses of 10–30 cm and granule conglomerate lags associated with trough cross-sets within 20–50 cm thick beds. (2) Nodular, very thinly bedded carbonaceous siltstone and shale with lignite breaks. This lithofacies comprises intervals approximately 2–5 m thick (Figure 4F–H). (3) Fine-grained, ripple cross-stratified sandstone with abundant plant debris and mud drapes in tabular beds (Figure 4G). Individual beds are less than 10 cm thick and comprise intervals that are 1–3 m thick (Figure 4F–H). The transition between siltstone and sandstone is typically gradational (Figure 4G).

4.2. Cantwell Formation Stratigraphy—Cabin Creek–Double Mountain Member
4.2.1. Representative Locations and Measured Sections

The Cabin Creek–Double Mountain member is well exposed in the Cabin Divide area, located immediately south of the Wyoming Hills (Figure 2), and at Double Mountain (DM1 in Figure 2). This mudstone-rich member is highly folded in the Cabin Creek area but is much less deformed in the Double Mountain area. Measured sections CAB01 (this study) and DM1 (Ridgway et al. [2]) serve as well-exposed examples of characteristic lithofacies, but do not record the total stratigraphic thickness of the member due to deformation and poor exposure in the more mudstone-rich sections.

4.2.2. Sedimentology

The Cabin Creek–Double Mountain member is characterized by thick sections of black-gray mudstone interbedded with sandstone packages of varying thickness (Figure 5A). All beds are laterally continuous and easily traced for hundreds of meters (Figure 5A). Sandstone beds occur as both 1–3 m thick packages interbedded within predominantly mudstone intervals, and as 5–7 m thick packages of more amalgamated sandstone with minor interbedded mudstone (Figure 5A,B). The thicker, more amalgamated sandstone packages consist internally of 10–30 cm thick beds of massive and ripple cross-stratified, medium-grained sandstone interbedded with massive and laminated mudstone intervals averaging ~0.5–1 m thick (Figure 5B). In the 1–3 m thick sandstone packages interbedded within intervals dominated by mudstone, bedding thickness diminishes from base to top, and the ratio of sand to shale decreases as shale breaks become more common (Figure 5C). In some sandstone packages, low-angle lateral accretion surfaces (see white triangles in Figure 5C) and minor internal scouring is observed. Broad, shallow erosional scours are most common in the thick, amalgamated sandstone packages.

Sandstone packages in the Cabin Creek–Double Mountain member consist of individual beds that are fine–medium-grained and massive at the base, and grade upward into wavy, flaser, and less commonly lenticular bedding (Figure 5D). In some cases, sandstone beds are bioturbated (Figure 5D) and contain soft-sediment deformational structures. The tops of most sandstone beds are dominated by symmetric ripples (Figure 5D,E); in rare cases, interference ripples are also preserved (Figure 5G). Fossilized wood fragments are commonly concentrated at the base of sandstone-dominated packages with minor coalified fragments interspersed (Figure 5H). Well-preserved leaf imprints are common in mudstone beds of any thickness.

Cyclicity between sandstone- and mudstone-dominated intervals is observed over the thickest exposed sections of the Cabin Creek–Double Mountain member. In Figure 5I, these cycles are bounded by ~5–7 m thick, amalgamated sandstone packages that stand out as the most resistant features of the exposure. The intervening thinner-bedded intervals have a gross thickness of ~15–25 m, are dominated by mudstone, and contain within them 1–3 m thick sandstone packages such as the package shown in Figure 5C. Other distinctive

lithofacies in the Cabin Creek–Double Mountain member are thin (<30 cm) limestone beds. Two types of limestone have been documented. The first type is a laminated limestone (Figure 5J). Individual laminae are crenulated and wispy with an individual thickness of less than 5 cm. The second type of limestone contains oncolites at the base and laminated limestone at the top of the bed (Figure 5K).

4.3. Correlation of Published Measured Sections

Here, we use the stratigraphic framework derived from our composite representative section of the Cantwell Formation to establish lithofacies correlations with previously published stratigraphic sections (Figure 6) (Trop [47]; Ridgway et al. [2]). We use the gradational contact between the Polychrome and Cabin Creek–Double Mountain members as a datum for comparison between sections. Note that the contact between the overlying Teklanika Formation and the Cantwell Formation is not a consistent datum for correlations as this contact is unconformable (Figure 6).

4.3.1. Correlation of the Polychrome Member

We correlate published stratigraphic sections from the base of Double Mountain (DM2), Fang Mountain (FM1), Mt. Sheldon (MS1), Refuge Valley (RV1), and the lower ~800 m of stratigraphy exposed at Panorama Mountain (PA1/PA2) with the Polychrome member (Figure 6). The feature most diagnostic of the base of the Polychrome member is conglomerate with abundant quartz clasts. An exception to this is the presence of limestone clasts and an absence of quartz clasts in conglomerate from sections near the southern basin margin, specifically Refuge Valley and Fang Mountain (Trop and Ridgway [2]). Each of these correlated sections consist of pebble–cobble conglomerate, sandstone, siltstone, and minor coal (Figure 6). Upward-fining trends are accompanied by similar changes in bedding geometry and sedimentary structures that match up-section changes observed in our composite representative section. Northward paleoflow indicators are dominant along the southern basin margin (PA1, RV1), southward indicators are dominant along the northern basin margin (MS1, DM2), and east/southeastward indicators are dominant in the central part of the basin (PC1) (Ridgway et al. [2]).

4.3.2. Correlation of the Cabin Creek–Double Mountain Member

We correlate the upper ~1000–1200 m of the previously published measured section PA1/PA2 at Panorama Mountain with the Cabin Creek–Double Mountain member (Figure 6). The upper part of section PA1/PA2 displays a prominent shift to 10–40 m thick sandstone packages interbedded with 10–50 m thick mudstone packages (FA3 and FA5 of Ridgway et al. [2]). In contrast to sections CAB01 and DM1, sandstone beds are commonly trough cross-stratified and mudstone packages are finely laminated, described by Ridgway et al. [2] as 'varve-like'. Despite these differences, we correlate this part of the stratigraphy at Panorama Mountain with the Cabin Creek–Double Mountain member because of the presence of thick mudstone packages and a clear lithofacies trend throughout section PA1/PA2 that we interpret to represent the gradational transition between members.

5. Depositional Environments of the Cantwell Basin

5.1. Polychrome Member

5.1.1. Lower Polychrome Member—Fluvial-Dominated Alluvial Fans

We interpret conglomerate-dominated intervals in the lower Polychrome member to represent deposition in fluvial-dominated or 'wet' alluvial fan systems [57,58]. Tabular, clast-supported conglomerate beds (Figure 4B) suggest deposition via sheet flood processes, where sediment is dispersed through unconfined flow from the mouths of proximal channels on alluvial fans e.g., Refs. [59,60]. Large average clast size (Figure 3) suggests an alluvial surface that was altered periodically by high-velocity flood events. Rapid sedimentation events on vegetated fan surfaces are supported by the documentation of upright tree fossils (Figure 4C), implying the deposition of several meters of sediment

relatively rapidly e.g., Ref. [61]. While conglomerate beds deposited via sheet floods are commonly imbricated [59], we interpret the general lack of both organization and imbrication of conglomerate in the lowest 180 m (PC1L in Figure 3) to suggest a more proximal fan position, where coarse sediment was transported in flashy, high-energy events (PC1L in Figure 7A) e.g., Ref. [62]. This interpretation is further supported by boulder-size clasts in the Polychrome member at PC1L.

5.1.2. Middle Polychrome Member—Braided Fluvial System

We interpret sandstone-dominated intervals characterized by trough cross-stratified sandstone and lenticular granule–pebble conglomerate beds with horizontal stratification to represent axial, braided-fluvial systems in the Cantwell basin (RC1 in Figure 7A). Conglomeratic lenticular bodies represent traction-based transport in active channels and on longitudinal barforms, whereas planar and trough cross-stratified sandstone represents the deposition of finer sediment on transverse barforms [63]. Thin-bedded, massive and horizontally stratified sandstone and interbedded siltstone are interpreted to represent overbank and floodplain deposits. Abundant leaf fossils suggest that subaerially exposed parts of bars and overbank environments were vegetated. Paleoflow indicators from the northern and southern basin margins [2,47] suggest that alluvial fans represented by the lower-middle Polychrome member were sourced from high topography on both sides of the basin, and that these systems merged into axial fluvial systems that drained the basin to the east, consistent with the depositional model of Ridgway et al. [2].

5.1.3. Upper Polychrome Member—Coastal Fluvial System

We interpret the upper Polychrome member to represent a transition to a coastal fluvial system with a vegetated floodplain (Figure 7B). Broadly channelized, medium–coarse-grained sandstone bodies suggest deposition within well-established channels with the tractive transport of sediment (Figure 4F). Tabular, thin-bedded ripple cross-stratified sandstone beds (Figure 4G,H) are interpreted to represent overbank deposits proximal to channels. Finally, thick carbonaceous siltstone and shale intervals (Figure 4F,H) are interpreted to represent a marshy overbank environment e.g., Ref. [64]. Thin lignite beds less than 5 cm thick indicate times of accumulation of organic matter atop a poorly developed soil profile and are often reworked as transported peat mats e.g., Ref. [65].
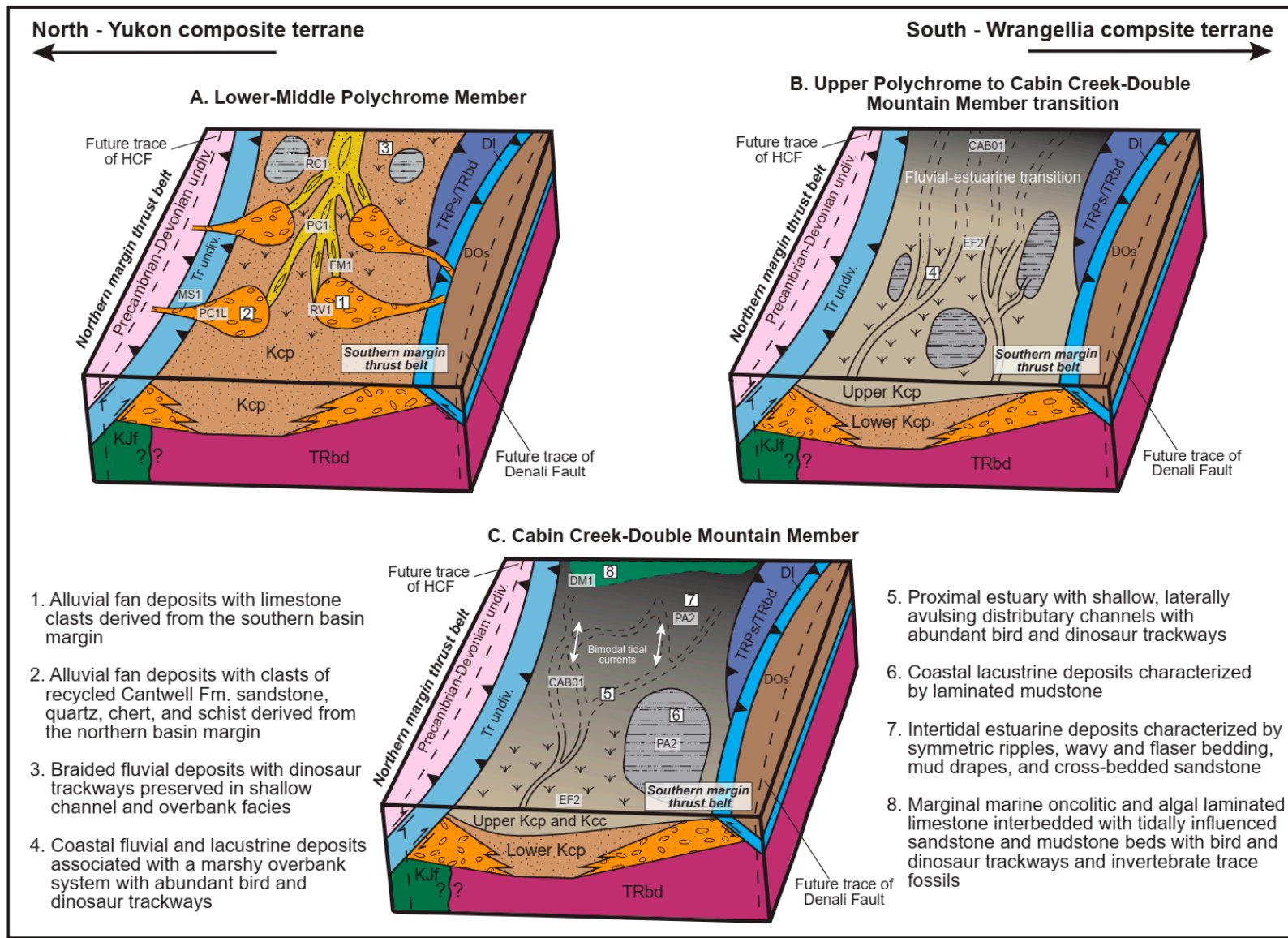
North - Yukon composite terrane

South - Wrangellia composite terrane

A. Lower-Middle Polychrome Member

B. Upper Polychrome to Cabin Creek-Double Mountain Member transition

C. Cabin Creek-Double Mountain Member

1. Alluvial fan deposits with limestone clasts derived from the southern basin margin

2. Alluvial fan deposits with clasts of recycled Cantwell Fm. sandstone, quartz, chert, and schist derived from the northern basin margin

3. Braided fluvial deposits with dinosaur trackways preserved in shallow channel and overbank facies

4. Coastal fluvial and lacustrine deposits associated with a marshy overbank system with abundant bird and dinosaur trackways

5. Proximal estuary with shallow, laterally avulsing distributary channels with abundant bird and dinosaur trackways

6. Coastal lacustrine deposits characterized by laminated mudstone

7. Intertidal estuarine deposits characterized by symmetric ripples, wavy and flaser bedding, mud drapes, and cross-bedded sandstone

8. Marginal marine oncolitic and algal laminated limestone interbedded with tidally influenced sandstone and mudstone beds with bird and dinosaur trackways and invertebrate trace fossils

Figure 7. Block diagrams illustrating a three-stage depositional model for evolution of the Cantwell basin. Numbers in white boxes refer to specific text points in the figure. (**A**) Deposition of the lower and middle Polychrome member. Fluvial-dominated alluvial fans are sourced locally from the northern and southern basin margins. The system transitions down-dip into an axial braided fluvial system. (**B**) Deposition of the upper Polychrome member and the transition to the lower Cabin Creek–Double Mountain member. The upper Polychrome member represents a coastal fluvial system with a heavily vegetated, marshy floodplain. The stratigraphic transition between the uppermost Polychrome member and lower Cabin Creek–Double Mountain member represents a proximal fluvial–estuarine transition zone with migrating distributary channels delivering sand to the estuary. (**C**) Estuarine and marginal marine depositional systems of the Cabin Creek–Double Mountain member. Coastal lacustrine systems are represented by finely laminated mudstones at Panorama Mountain. Oncolitic and algal laminated limestone bed interbedded with dinoflagellate and acritarch-bearing mudstone are indicative of a brackish, marginal marine depositional system at Double Mountain [2].

5.2. Cabin Creek–Double Mountain Member

We interpret the Cabin Creek–Double Mountain member to represent a tidally influenced marginal marine depositional system that included estuarine and coastal lacustrine environments (Figure 7B,C). Note that our interpretation of an estuarine environment does not necessarily invoke a relationship with an incised paleovalley and related embayment, rather the use of the term is intended to refer generally to a transgressive estuarine system e.g., Ref. [66]. The Cabin Creek–Double Mountain member is characterized by heterolithic intervals dominated by wavy and flaser bedding, mud drapes on internal beds within sandstone packages, and symmetric ripples. The flaser-bedded sandstone, defined by discontinuous mud drapes in ripple cross-stratified sandstone, and the wavy-bedded sandstone (Figure 5D), defined by continuous mud drapes in ripple cross-stratified sandstone, both reflect abrupt changes in flow velocity that allow the deposition of markedly different grain sizes. These types of sedimentary structures are common in modern estuarine depositional systems within intertidal zones where ripple cross-stratified sandstone is deposited during the maximum flow velocities associated with dominant tidal periods, whereas silt and mud settle out of suspension during slack-water periods [67,68]. These diagnostic sedimentary structures are more common at Double Mountain than Cabin Creek, which we interpret to reflect a more proximal part of the estuarine system preserved at Cabin Creek relative to Double Mountain. In many estuarine systems, tidal currents are often strongest in medial positions where water depths remain shallow, but the influence of fluvial processes and direct sediment input is minimal [66]. Symmetric ripples are abundant in all sandstone packages (Figure 5E,F) and are interpreted as a product of bi-directional tidal currents re-working sand deposited in distributary channels and as part of tidal bars. Interference ripples (Figure 5G) are far less common and most likely formed in specific locations where subordinate currents disrupted the dominant bi-directional current, overprinting the primary symmetric ripples that are ubiquitous throughout the section e.g., Ref. [69].

The 5–7 m thick amalgamated sandstone packages consist of mostly massive and ripple cross-stratified sandstone beds with broad internal scours and are interpreted to represent primary distributary channels within the estuarine system. When active, these distributary channels were where most of the sand in the system was deposited and frequently reworked e.g., Ref. [66]. The cyclicity that is highlighted by the occurrence of an amalgamated sandstone package every ~25 m (Figure 5I) is interpreted as the product of avulsion processes where the depositional axis migrated laterally across the estuary. Low-angle lateral accretion surfaces were observed in sandstone packages of varying thickness and are interpreted as evidence of laterally migrating point bars formed within these constantly evolving distributary channels [66]. The 1–3 m thick sandstone packages within mudstone-dominated intervals are interpreted to represent off-axis parts of the system where shallow, short-lived distributary channels formed when sand was routed

from the main depositional axis, and mudstone was deposited at times when there was an absence of sand input and corresponding lower energy.

At Cabin Creek, there is an absence of obvious trace fossils, but burrows are common at the Double Mountain section. It is possible that these features were not well preserved in the Cabin Creek area due to the extensive deformation that these strata have experienced in the footwall of the Cabin Creek fault (see Section 6). Alternatively, the absence of burrowing organisms may reflect particularly harsh conditions in the depositional environment during the deposition of the Cabin Creek section. The fluvial–tidal transition is often a particularly challenging environment for biological life to thrive due to frequent re-working of the sediment substrate and variable salinity, including seasonal variations e.g., Ref. [66]. The more common bioturbation in the Double Mountain section may be a function of more stable salinity levels in what we interpret to have been a more medial part of the estuarine system. This interpretation would be consistent with the documentation of several species of dinoflagellates, suggestive of more brackish marine conditions at Double Mountain [2]. The thin limestone beds best developed at Double Mountain are interpreted as algal-influenced limestones. The laminated limestone beds with crenulated lamina (Figure 5J) are interpreted to represent amalgamated algal mats e.g., Refs. [70–72]. The oncolitic limestones (Figure 5K) represent deposition when the algal material accumulated around a nucleus that was periodically transported in the intertidal zone e.g., Ref. [73].

Like modern estuarine-dominated coastlines, we interpret the Late Cretaceous estuarine systems of the Cantwell Formation to have been laterally adjacent to lacustrine systems. Sedimentologic data for lacustrine depositional systems is best documented from the previously published measured section at Panorama Mountain (Figure 6) [2]. At this location, interbedded with the heterolithic intervals are 10–50 m thick packages of laminated mudstone with millimeter-scale laminations rich in plant fragments. These types of sedimentary structures reflect an exceptionally calm environment within which suspension deposition dominated for long periods of time (Figure 7C). Trough cross-stratified sandstone bodies associated with the laminated mudstone packages likely represent times when coarse sediment prograded into lacustrine environments from the outlets of fluvial channels, possibly within small, prograding deltas e.g., Ref. [74].

The basin-scale shift from alluvial–fluvial systems in the Polychrome member to marginal marine and lacustrine systems in the Cabin Creek–Double Mountain member represents a long-lived transgression. Ridgway et al. [2] interpreted marginal marine influence in the uppermost Cantwell Formation to be part of the Bearpaw transgression. The Bearpaw transgression has been documented in several locations in North America as a diachronous transgression throughout the North American Cordillera and other parts of Late Cretaceous Euramerica e.g., Refs. [2,75–77]. Overall, our depositional model remains consistent with this general interpretation, though more robust chronostratigraphic control would be required to relate the specific timing of transgression in the Cantwell basin to other stratigraphic sections in the Cordilleran foreland basin system where the Bearpaw transgression has been better documented. An alternative, more local driver of the transgression recorded by the Cantwell Formation may be increased subsidence resulting from loading of the crust by syndepositional thrust systems that bordered the basin.

5.3. Stratigraphic Context of Trace Fossils in the Cantwell Formation

Our depositional model also provides stratigraphic context to important paleontological datasets, especially bird and dinosaur trackways in Denali National Park and Preserve. The most prolific dinosaur tracksites described in the literature are associated with fluvial strata of the middle-upper Polychrome member, most notably in the Tattler/Igloo Creek region (Figures 2 and 7A,B). This part of the basin has yielded numerous theropods and hadrosaur trackways, the first pterosaur manus trackway found in Alaska, and the northernmost occurrence of a therizinosaur e.g., Refs. [14,16,17,78]. Also of note are numerous documented trackways and feeding traces of wading birds (Aquatilavipes swiboldae, Ignotornis mcconnelli, Magnoavipes denaliensis, Gruipeda vegrandiunus, and Uhangrichnus

chuni), which are most common in strata of the uppermost Polychrome member and the lower Cabin Creek–Double Mountain member (Figure 7B) [4,18,78]. This record of wading birds is important because it provides insight into the paleobiology of the coastal fluvial and estuarine/lacustrine depositional systems that formed through transgression in the Cantwell basin. Similar wading birds in modern estuarine and tidal flat environments often take advantage of low tide to feed in the intertidal zone. Trackways in these environments have especially high preservation potential as new sediment is deposited rapidly by the next high tide e.g., Ref. [79].

6. Structural Configuration

6.1. Geologic Mapping and Structural Observations

Our mapping and compilation work was focused primarily on the Toklat River corridor and the northern margin of the Cantwell basin between the Toklat River and the East Fork of the Toklat River (Figure 2). The results of this compilation and our strike and dip measurements along the Toklat River corridor are shown in Figure 8A. The inset map shown in Figure 8B is a detailed map of the northern margin of the study area. Numbered locations in both maps are referenced in the text to indicate the locations where key structural observations were made in the field.

6.1.1. Thrust System along the Northern Basin Margin

The Cantwell Formation along the northern basin margin is deformed within a previously undocumented, south-verging thrust system (Figure 8). The Cabin Divide fault (CDF) marks the northern margin of the continuous exposures of the Cantwell Formation within this system and juxtaposes Jurassic–Cretaceous metasedimentary strata (unit KJf) against Upper Cretaceous strata of the Cantwell Formation (Location 1, Figures 8A,B and 9). The dip of the CDF is difficult to constrain since the fault is mostly covered in a valley. Thus, we did not alter the trace of the fault as shown in the original linework of Gilbert and Redman [36], which depicts the fault as a steeply south-dipping normal or oblique-slip fault. However, based on the following structural characteristics of the Cantwell Formation just to the south, it is apparent that the CDF must have accommodated south-verging, contractional deformation, at least during the deformation of the Cantwell Formation. Open folds in the Polychrome member south of the CDF verge to the south–southeast with approximately east–west trending axial traces (e.g., Location 2 in Figure 8B; folds also shown in a field photo in Figure 8C). Reverse faults associated with these folds dip approximately 40–45° to the north and typically break through anticlines slightly fore of the fold hinge. Based on this observation and the fold geometries, we interpret the folds that deform the Polychrome member as fault propagation folds. Upper Paleocene–Lower Eocene volcanic strata of the Teklanika Formation unconformably overlie folded strata of the Cantwell Formation within the northern margin thrust belt and are most extensively preserved in synclines (Figure 8C). Folds in the Teklanika Formation are lower amplitude and disharmonic relative to folds in the Cantwell Formation (Location 3 in Figures 8B,C and 9B).

In the shale-rich Cabin Creek–Double Mountain member, fold geometries range from open to tight with angular hinges, including chevron-style folds. Local thickness changes are common in deformed shale beds, particularly near and within fold hinges. The axial planes of folds in this part of the Cantwell Formation are typically subvertical and trend roughly east–west. While the difference in deformational style observed between the shale-rich and sandstone/conglomerate-rich strata in the Cantwell Formation may be attributable to lithology, it is also possible that folds in the upper part of the section record a component of detachment folding e.g., Ref. [80], though we cannot fully assess this option based on our data.
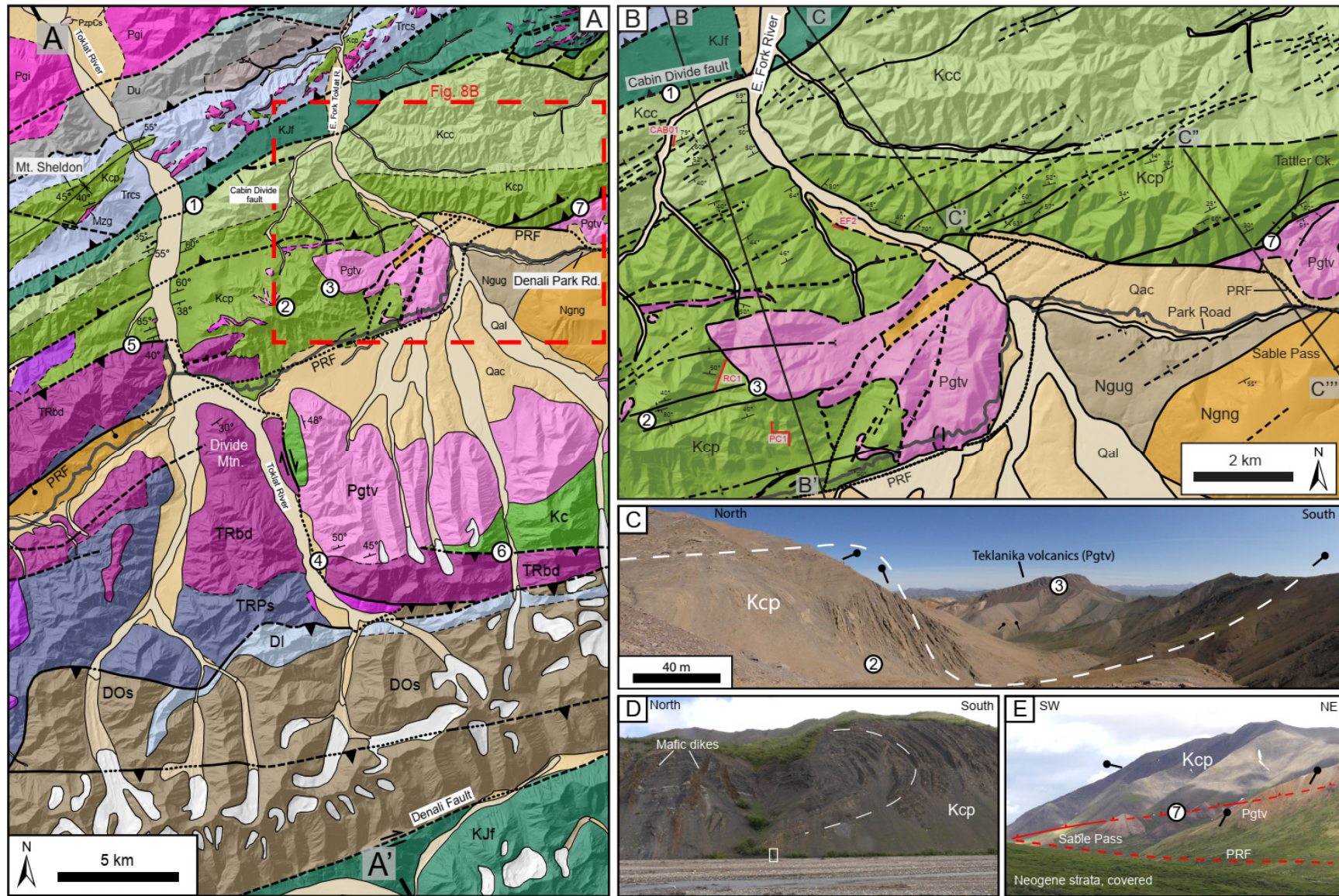
Figure 8. (**A**) Geologic map of the study area in the western Cantwell basin. The areal extent of this map is shown by the white dashed rectangle in Figure 2. Strike and dip symbols represent data collected from field traverses along the Toklat River corridor. Key elements include a north-verging thrust fault that carries unit TRbd over the lower-middle Polychrome member (Location 5). Movement of this thrust sheet is accommodated by a tear fault just east of the Toklat River, which juxtaposes the Teklanika Formation and unit TRbd (Location 4). See the legend in Figure 2 for unit abbreviations and colors. (**B**) Detailed geologic map of the northern basin margin between the Toklat River and Tattler Creek. The areal extent of this map is indicated by the red dashed rectangle in (**A**). Strike and dip measurements and fold axial traces are compiled from our field mapping and the data of Gilbert and Redman [36]. The locations of measured sections that comprise our composite representative section (Figure 3) are shown in red. See the legend in Figure 2 for unit symbols and colors. (**C**) Field photograph of a fault propagation fold in the Polychrome member (Kcp) overlain by the Teklanika Formation (Pgtv). The dashed white line traces bedding and black tadpole symbols show the orientation of bedding. Note that the corresponding relationships in the cross-section in Figure 9B appear slightly different as the photograph was taken from along strike of the cross-section line. (**D**) Field photograph of an overturned, reclined anticline exposed along the east bank of the East Fork of the Toklat River in the middle-upper Polychrome member. Mafic dikes cross-cut stratigraphy at a high angle in the backlimb. Apparent dip resulting from an approximately 15° difference in the orientation of the outcrop face relative to the profile plane of the fold has resulted in this fold being described as "recumbent" in previous publications. A person for scale in the white box. (**E**) Field photograph taken looking northwest at Sable Pass and the south side of Sable Mountain shows the Teklanika Formation (Pgtv) in the footwall of the frontal south-verging reverse fault of the northern margin thrust system. The middle-upper Polychrome member is exposed in the hanging wall. The Park Road fault (PRF) runs through the pass itself. A–A′, B–B′ and C′–C‴ represent the indication of the location of the line of section.
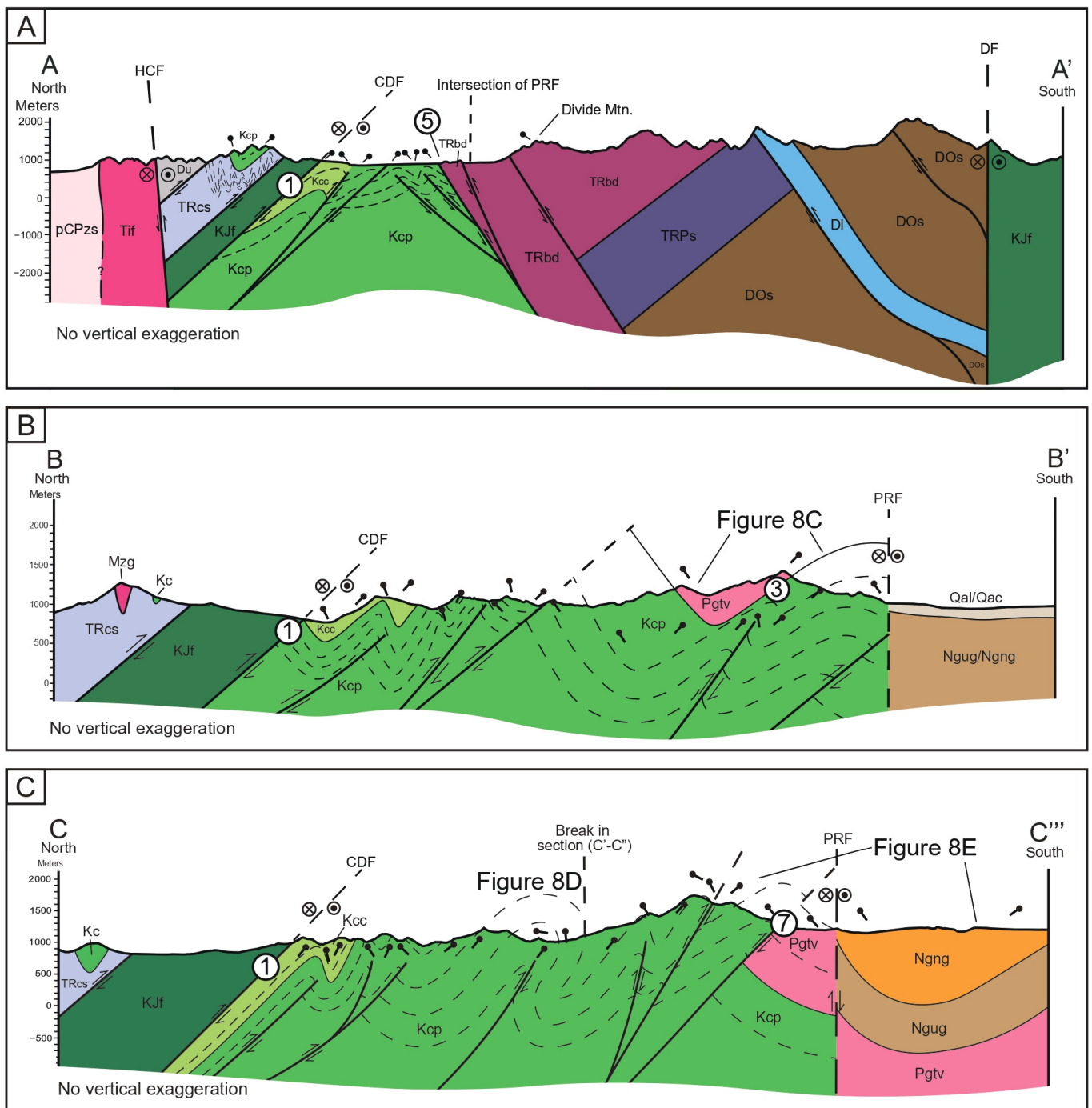
Figure 9. Geologic cross-sections through key parts of the study area in the western Cantwell basin. The locations of the cross-sections are marked in Figure 8. (**A**) Generalized geologic cross-section from A–A′. The Cantwell Formation is deformed by opposing thrust faults along the northern and southern basin margins. (**B**) Geologic cross-section from B–B′. Fault propagation folds in the southern part of the cross-section are disharmonic relative to an open syncline in the Teklanika Formation. The shale-rich upper Polychrome member and Cabin Creek–Double Mountain member are deformed in tight chevron folds in the footwall of the Cabin Divide fault (CDF) (Location 1). The frontal part of the south-verging thrust belt is truncated by the Park Road fault (PRF). The location of the field photograph shown in Figure 8C is marked on this cross-section. (**C**) Geologic cross-section from C–C‴. The frontal reverse fault of the south-verging system places the Polychrome member (Kcp) over the Teklanika Formation (Pgtv) (Location 7). The Park Road fault (PRF) passes through Sable Pass with Neogene strata exposed south of the fault. The location of the field photographs shown in Figure 8D,E are marked on this cross-section.

6.1.2. Thrust System along the Southern Basin Margin

The southern basin margin is defined by a north-verging thrust system involving Ordovician–Triassic marine strata for tens of kilometers along strike (units DOs, Dl, TRPs, and TRbd, Figures 2 and 8A). North-verging thrust sheets are particularly well exposed along the upper Toklat River corridor (Figure 8A). A key structure associated with this system is a north–south-trending tear fault along the east bank of the upper Toklat River (Location 4 in Figure 8A). The leading reverse fault along the northern edge of the thrust sheet bounded by the tear fault places Upper Triassic basalt (TRbd) over the Polychrome member (Kcp) (Location 5 in Figures 8A and 9A). The tear fault itself truncates a depositional contact between the Teklanika Formation (Upper Paleocene–Lower Eocene) and unit TRbd at location 4 (Figure 8A). This relationship contrasts with location 6, just 5 km to the east, where the Cantwell Formation is in fault contact with unit TRbd (Figure 8A).

6.2. Interpretation of Deformational Timing

Syn- and post-depositional contraction influenced alluvial systems along the basin margins and resulted in the deformation of the Cantwell Formation during and soon after deposition. During the deposition of the Cantwell Formation, high topography within the active, basin-bounding thrust belts provided proximal sources of sediment such as quartz and schist clasts along the northern basin margin and diagnostic limestone clasts along the southern basin margin. Basinward propagation of the thrust belts early in the deposition of the Cantwell Formation is evident from the presence of eroded, lithic-rich coarse-grained sandstone of the lowermost Polychrome member re-deposited as clasts in conglomerate beds of the upper-lower to middle Polychrome member, cf. [81]. Ridgway et al. [2] also documented growth unconformities along the southern basin margin near Panorama Mountain (PA1/2 in Figure 2), which clearly record this process of the syn-kinematic deposition of alluvial fan strata along the active margins of the basin. Additional evidence of the basinward propagation of the northern margin thrust belt is the structural isolation of part of the lower Polychrome member at Mt. Sheldon (Figure 8A). In this location, the basal cobble–boulder conglomerate of the Polychrome member unconformably overlies Upper Triassic marine strata (TRcs in Figures 2 and 8A) and is folded in the core of an open syncline. This exposure is isolated to the north of the CDF, though the timing of its isolation is unclear as younger strata of the Cantwell Formation may have been deposited and subsequently eroded as the northern basin margin was uplifted.

The volcanic eruptions that produced the Teklanika Formation had commenced by the Late Paleocene [10,46] and coincided with the continued shortening of the Cantwell basin. The contact between the Cantwell Formation and Teklanika Formation is locally an angular unconformity, and the Teklanika Formation is deformed by lower amplitude, more open folds relative to the Cantwell Formation. The most complete sections of the volcanic strata are preserved in synclines in the Cantwell Formation. We interpret these relationships to reflect the syn-deformational deposition of the Teklanika Formation following significant unroofing of parts of the Cantwell Formation, such as at location 3 where the Teklanika Formation is deposited over part of the middle-lower Polychrome Member (Figure 8B,C). Further evidence for contractional deformation following deposition of the Teklanika Formation includes two key field relationships: (1) at location 7, an east–west-trending, south-verging reverse fault at the frontal edge of the northern thrust belt places the Cantwell Formation over the Teklanika Formation (Figures 8B,E and 9C); and (2) at location 4, the tear fault along the upper Toklat River corridor truncates the contact between the Teklanika Formation and underlying Triassic basalt (Figure 8A). Though not the focus of this study, evidence for the post-Eocene overprinting of contractional structures in the Cantwell basin is abundant. One of the better examples is the Park Road fault (PRF), first documented and informally named by Gilbert and Redman [36]. This fault roughly coincides with the location of the Park Road through the middle third of the road, truncating the frontal edge of the south-verging northern margin thrust belt (Figure 8A). This structure appears to

behave like well-described strike-slip faults that often change along strike from extension to strike-slip to contraction over relatively short distances e.g., Ref. [82].

7. Provenance of the Cantwell Basin

7.1. U-Pb Detrital Zircon Geochronology Results

Analysis of detrital zircon populations for 13 samples from the Cantwell Formation allows for the reconstruction of regional sediment pathways into the basin and provides new insights into the paleogeographic setting of the Cantwell basin. The stratigraphic locations of the detrital zircon samples are shown in Figures 3 and 6. Since there is very little relative variation in the age spectra of samples from each respective member, we present composite probability density plots (PDPs) for each member in Figure 10 (PDPs for each sample are available in Supplementary File S2).
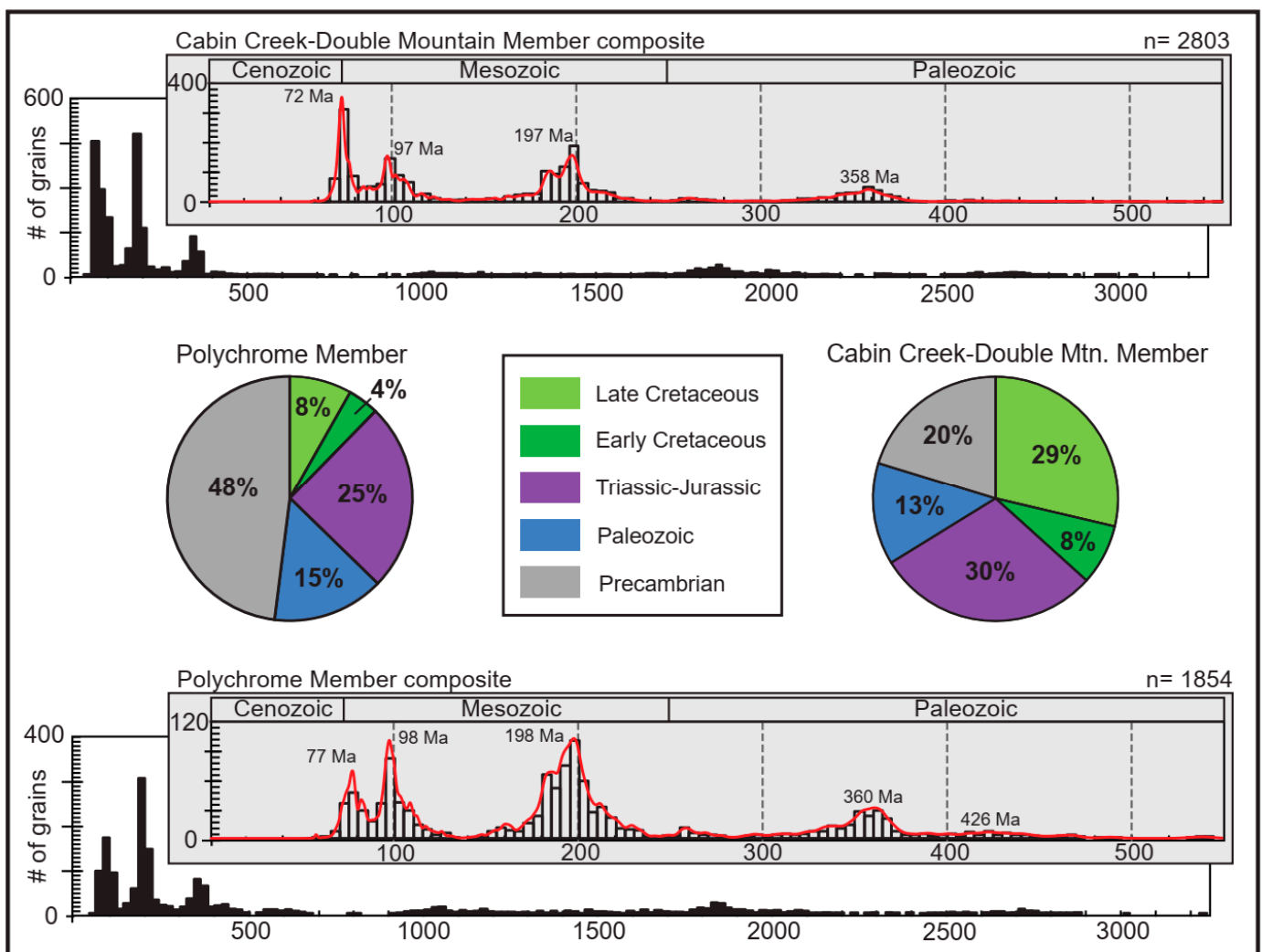
Figure 10. Composite probability density plots showing U-Pb detrital zircon spectra for the Polychrome and Cabin Creek–Double Mountain members. The inset plots show ages from 550 to 0 Ma with the probability density function displayed as a red curve over the histogram. Pie charts show the proportions of Late Cretaceous, Early Cretaceous, Triassic–Jurassic, Paleozoic, and Precambrian U-Pb ages from both members. The Cabin Creek–Double Mountain member includes a greater proportion of Late Cretaceous grains and fewer Precambrian grains relative to the Polychrome member.

7.1.1. Polychrome Member

Eight detrital zircon samples (n = 1854) from the Polychrome member yield dominant Phanerozoic populations that consist of Devonian–Mississippian, Triassic–Jurassic, and Cretaceous grains (Figure 10). Triassic–Jurassic grains comprise the most abundant Phanerozoic population with ages between ca. 240 and 150 Ma and account for 25% of all grains. Early and Late Cretaceous populations account for 4% and 8%, respectively (Figure 10). Paleozoic grains account for 15% of all grains and are dominated by a population between ca. 375 and 300 Ma. Precambrian grains constitute 48% of the age spectra. The Precambrian grains span a wide range of ages with the greatest proportions of grains between 1200 and 950 Ma and 2000 and 1800 Ma (Figure 10).

7.1.2. Cabin Creek–Double Mountain Member

Five samples from the Cabin Creek–Double Mountain member (n = 2803) yield nearly all the same dominant populations as the Polychrome member, though a significantly higher proportion of Late Cretaceous grains are concentrated within the youngest population between ca. 77 and 66 Ma (Figure 10). Early and Late Cretaceous grains are more abundant relative to the Polychrome member, comprising 8% and 29%, respectively (Figure 10). A total of 30% of grains yield Triassic–Jurassic ages, and 13% yield Paleozoic ages (Figure 10). The Cabin Creek–Double Mountain member includes a smaller proportion of Precambrian grains (20%) relative to the Polychrome member with similar common populations. Our raw data include ten ages slightly younger than Late Cretaceous, which we attribute to Pb loss based on the correlation with the timing of peak magmatism at 57 Ma [10], along with no existing age control to suggest that any part of the Cantwell Formation was deposited after the Maastrichtian.

7.2. Detrital Zircon Provenance Interpretation

Comparison of detrital zircon ages from the Cantwell Formation with published ages and locations for potential primary (igneous) and secondary (meta)sedimentary sources yields the following insights:

(1) The youngest population (ca. 77–66 Ma) overlaps with the deposition of the Cantwell Formation and was derived from a coeval magmatic arc system located south of the basin.

(2) Cretaceous grains with ages that precede the deposition of the Cantwell basin were derived from older exhumed Cretaceous plutons exposed throughout south-central Alaska, primarily south of the Cantwell basin.

(3) Sediment was recycled from Paleozoic and Mesozoic metasedimentary strata that were locally uplifted in syndepositional thrust systems along the southern and northern basin margins.

(4) Sediment was recycled from Jurassic–Cretaceous sedimentary sources that were exhumed in a Cretaceous suture zone presently exposed south of the basin.

(5) Precambrian grains were recycled from metamorphic rocks exposed north of the Cantwell basin that represent the ancestral North American margin.

For brevity, we have summarized our provenance interpretations in Table 1, along with key references.

Table 1. Summary of detrital zircon provenance interpretations for primary and secondary (recycled) sources and relevant references.

	Provenance Interpretation	Source Ages/Location	References
Primary Sources	Active Late Cretaceous magmatic arc	**110–55 Ma**: Plutons exposed in the central and western Alaska range **70–50 Ma**: Upper Cretaceous–Eocene plutons exposed in the eastern Alaska range	Jones et al. [83]; Koeneman and Wilson [84]; Moll-Stalcup [85]; Reed and Lanphere [86,87]; Lanphere and Reed [88]; Wallace and Engebretson [89] Moll-Stalcup [85] and references therein; Wilson et al. [90]
	Early and Late Cretaceous plutons of the Alaska Range	**110–85 Ma**: Plutons exposed in the eastern Alaska range – some are intruded into the Yukon composite terrane	Moll-Stalcup [85] and references therein; Wilson et al. [90]
	Taylor Mountain Batholith	**216–181 Ma**: Plutons exposed in eastern Alaska — intruded into the Yukon composite terrane	Day et al. [91]; Dusel-Bacon and Williams [92]
	(Meta)plutonic rocks of the Yukon composite terrane	**380–330 Ma**: Orthogneiss — eastern Alaska and Yukon **365–320 Ma**: Quesnellia and Slide Mountain terranes — Yukon and B.C.	Aleinikoff et al. [93]; Day et al. [94]; Dusel-Bacon and Aleinikoff [95]; Dusel-Bacon et al. [96,97]; Johnston et al. [98]; Mortensen [99]; Nelson et al. [100] Greig and Gehrels [101]; Johnston et al. [98]; Mortensen [99]
Secondary Sources	Recycled sediment from the Kahiltna assemblage	**Northern belt**: sediment derived primarily from the Yukon composite terrane (ancestral North American margin) **Southern belt**: sediment derived primarily from the Wrangellia composite terrane (includes arc sources listed below)	Kalbas et al. [102]; Hampton et al. [42,103]; Hults et al. [104]; Box et al. [43]; Romero et al. [40]
	Talkeetna arc *	**201–153 Ma**: Peninsular terrane — south-central Alaska	Pálfy et al. [105]; Amato et al. [106]; Rioux et al. [107–109]
	Chitina arc *	**175–135 Ma**: Wrangellia terrane — south-central Alaska	Nokleberg et al. [110]; Plafker et al. [111]; Roeske et al. [112]; Day et al. [113]; Beranek et al. [114]
	Chisana arc *	**140–115 Ma**: Wrangellia terrane — south-central Alaska	Snyder and Hart [115]; Graham et al. [116]
	Recycled from thrust sheets along basin margins	**Key populations: 700–400 Ma and 1000–900 Ma**	Keough and Ridgway [45]
	Recycled from the Yukon composite terrane	**Key populations: 2800–2600 Ma, 2000–1800 Ma, and 1100–1000 Ma**	Dusel-Bacon et al. [117]; Ross [118]; Rainbird et al. [119]; Romero et al. [40], and references therein

* Arc sources interpreted in the Cantwell Formation as recycled from the Kahiltna assemblage
Note: Colors for primary sources correspond to colored bands in Figure 11 which represent these sources

We also refer the reader to detailed compilations of regional detrital zircon sources documented for strata exposed in the central Alaska Range by Hampton et al. [42,83], Brennan and Ridgway [120], Lease et al. [121], and Romero et al. [40], and in the western Alaska Range by Box et al. [43].

7.2.1. Paleogeographic Insights from Provenance Interpretations

Late Cretaceous detrital zircon ages between ca. 75 and 66 Ma overlap with the Campanian–Maastrichtian biostratigraphic age ranges based on palynology of Ridgway et al. [2], and with U-Pb ages of bentonites interbedded within the Cantwell Formation e.g.,

Refs. [3,8,11,18]. This overlap suggests that there was an active silicic volcanic source supplying sediment to the basin during the deposition of the Cantwell Formation (Figure 11). The coeval magmatic arc system was located south of the Cantwell basin (present day coordinates) and is represented by plutons exposed throughout the Alaska Range (Figures 1 and 12; Table 1). The youngest part of the arc consists of plutons mostly less than 75 Ma and is well exposed in the western Alaska Range, south of the Denali fault (Figure 1) [83]. Restoration of ~480 km of dextral displacement on the Denali fault [41,122–124] places these plutons proximal to the southern margin of the Cantwell basin. While grains derived from the active arc are present in all samples from the Cantwell Formation (Figure 9), we observe a marked increase in the proportion of Late Cretaceous grains in the Cabin Creek–Double Mountain member of the Cantwell Formation. We interpret the increase in Late Cretaceous grains to record an uptick in magmatism, consistent with magmatic ages from the arc (Figure 11) [83].
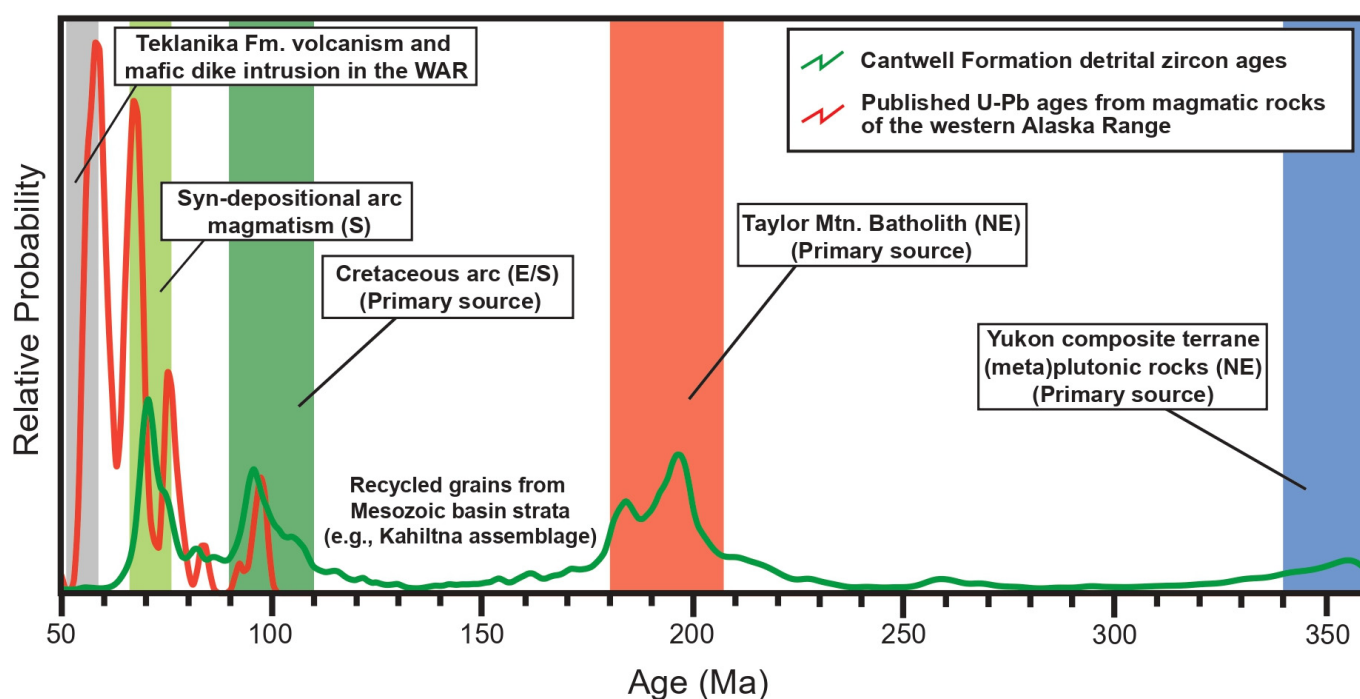
Figure 11. Normalized PDP plots showing U-Pb detrital zircon ages from the Cantwell Formation (green curve) vs. U-Pb magmatic ages from the western Alaska Range (red curve; Jones et al. [83] and references therein). Latest Cretaceous detrital zircon ages overlap with a period of increasing magmatic intensity in the arc, which was located south of the Cantwell basin during the time of deposition. Colored bands delineate key time intervals that correspond with interpreted primary sources for detrital zircons in the Cantwell Formation. The gray band corresponds to the timing of regionally extensive magmatism represented in the study area by the Teklanika Formation. Abbreviated cardinal directions in parentheses indicate the paleo-position of each source relative to the Cantwell basin using modern coordinates. WAR—Western Alaska Range.

North of the Cantwell basin, parts of the Yukon composite terrane (ancestral North American margin) comprised topographic highs during the Late Cretaceous, including a regional anticlinorium proximal to the northern margin of the basin (Figure 12) [2,125]. We interpret significant sediment contribution from this region to the Cantwell basin. For example, all detrital zircon samples from the Cantwell Formation, regardless of geographic or stratigraphic location, yield a significant population between ca. 220 and 180 Ma (Figures 10 and 11). We interpret these grains to reflect plutonic sources located northeast of the Cantwell basin, the most proximal of which is the Taylor Mountain batholith (TMB) (Table 1). The TMB intruded into the Yukon composite terrane, and published magmatic

ages range from 216 to 181 Ma. This age range accounts for 23% of grains in the Cantwell Formation. Evidence for much more proximal sources of sediment from the YCT includes the presence of abundant quartz and schist clasts in conglomerate of the lower Polychrome member along the northern basin margin. These conglomerate beds are also associated with southward paleoflow indicators [2,81].
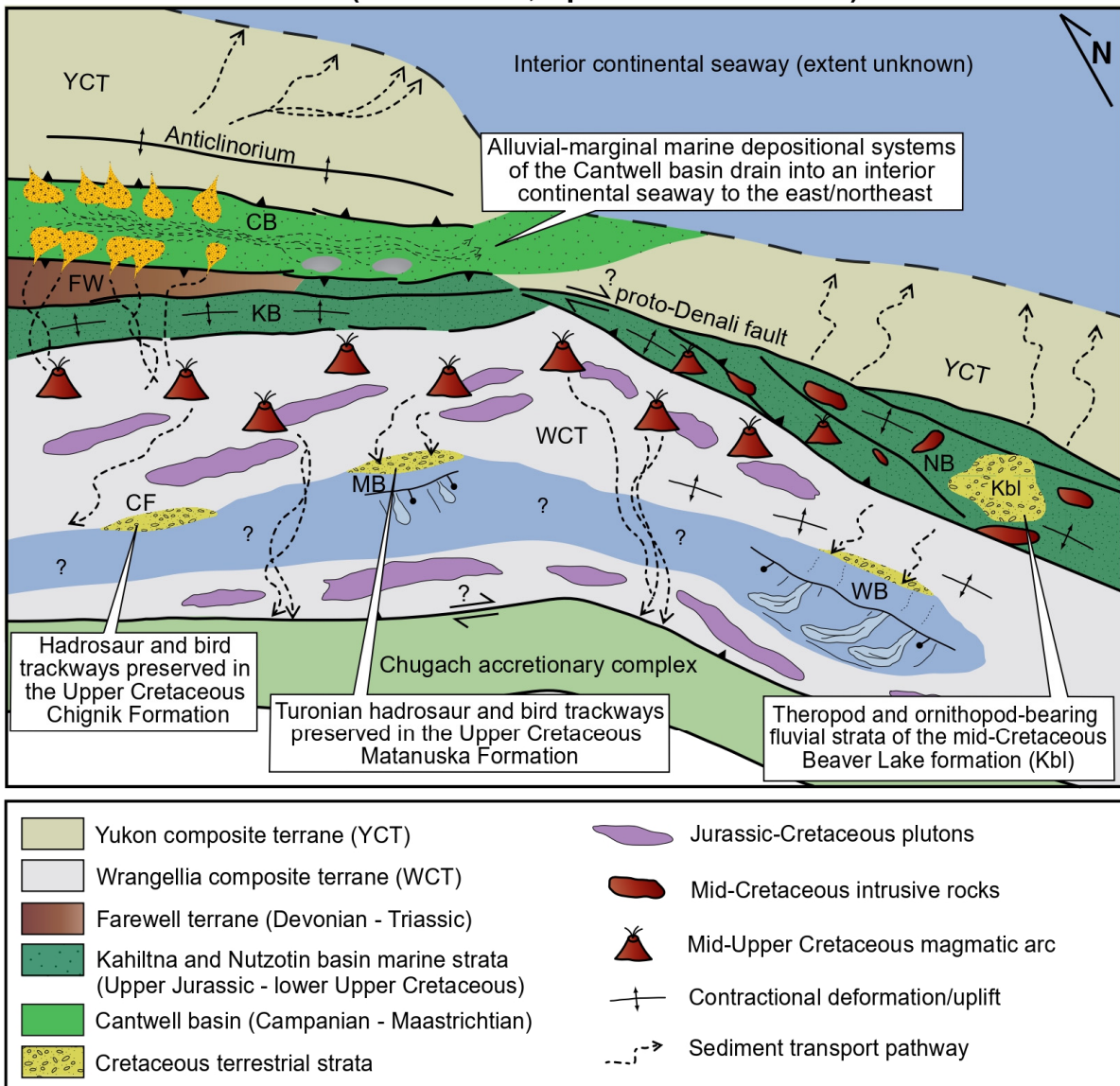
Mid to Late Cretaceous (~120–70 Ma, Aptian–Maastrichtian)

Figure 12. Simplified Mid to Late Cretaceous paleogeographic map (modified from Trop et al. [126], after Trop and Ridgway [44]). The sketch shows current locations of Cretaceous terrestrial strata and does not account for up to 500 km of Cenozoic strike-slip displacement on the Denali fault [41,122–124]. The Cantwell basin is bordered to the south by an active magmatic arc and deformed and uplifted marine strata of the Kahiltna basin (KB) and Farewell terrane (FW). Forearc basin strata include the Matanuska basin (MB), Chignik Formation (CF), and Wrangell Mountains basin (WB). Proximal foreland basin depocenters are represented by the Cantwell basin (CB) and the Beaver Lake formation (Kbl). The Beaver Lake formation contains dinosaur trackways and was deposited over deformed marine strata of the Nutzotin basin (NB). The Cantwell basin is interpreted to have connected to an interior continental seaway, the extent of which is unknown.

7.2.2. Regional Sediment Recycling

7.2.2.1. Recycling of the Kahiltna Assemblage

We interpret a portion of the dominant detrital zircon populations in the Cantwell Formation to have been recycled from sedimentary strata of the Upper Jurassic–Cretaceous Kahiltna assemblage (Table 1; Figures 11 and 12). The Kahiltna assemblage is exposed throughout the central and western Alaska Range, as well as the northern Talkeetna Mountains (Figure 1). Since most Early Cretaceous and older grains in the Cantwell Formation overlap with dominant populations in the Kahiltna Assemblage, it is difficult to accurately interpret its significance as a secondary sediment source versus both units being sourced from the same primary sources. However, there are minor, yet unique populations present in the Cantwell Formation that were almost certainly recycled from the Kahiltna assemblage. Specifically, the Talkeetna, Chisana, and Chitina arcs that were built on the Wrangellia composite terrane are the most likely sources for grains between ~175 and 135 Ma in the Cantwell Formation (Table 1). From a paleogeographic perspective, it is most easily reconciled to have these specific zircons recycled from the more proximal Kahiltna assemblage rather than the more distal exposures of the plutons representing these three arc systems. It is important to note that reconstruction of ~480 km of dextral displacement on the Denali fault system places the Kahiltna assemblage now exposed in the western Alaska Range directly south of the Cantwell basin.

7.2.2.2. Recycling Driven by Syndepositional Exhumation of the Cantwell Basin Margins

Minor detrital zircon populations between ca. 700 and 400 Ma (n = 112) and 1000 and 900 Ma (n = 20), observed primarily in the Polychrome member (Figure 10), are unique to metasedimentary strata exposed in the syndepositional thrust sheets that border the Cantwell basin (Table 1; Figures 2, 8 and 9). Specific map units include Devonian–Ordovician and Permian–Middle Triassic marine strata (DOs and TRPs in Figure 2), Upper Triassic marine strata (TRcs in Figure 2), and Upper Jurassic–Lower Cretaceous marine strata (KJf in Figure 2) e.g., Refs. [33,34,127]. U-Pb detrital zircon ages from these strata include late Mesoproterozoic, Neoproterozoic, and Silurian–Ordovician populations that are extremely uncommon in rocks of the YCT or Wrangellia composite terrane [45]. Note that while unit KJf in the study area has been interpreted by regional mapping studies as part of the Kahiltna assemblage [34], recent U-Pb detrital zircon analyses from unit KJf along the northern basin margin yielded age spectra that are distinct from strata of the Kahiltna assemblage exposed south of the Denali fault [45]. Direct sediment input from basin-bounding thrust systems during the deposition of the Cantwell basin is also consistent with conglomerate clast compositions in alluvial fan strata along both margins documented in previous studies [2,81]. For example, limestone clasts common in conglomerate along the southern margin of the Cantwell basin can be directly linked to Upper Devonian sources (Dl in Figures 2 and 8A) in the southern thrust system based on conodont assemblages [2].

7.2.2.3. Regional Sediment Recycling from the Yukon Composite Terrane

Precambrian populations comprise significant components of the age spectra for the Polychrome member (48%) and the Cabin Creek–Double Mountain member (20%) (Figure 10). We interpret the more common populations of 1100–1000 Ma, 2000–1800 Ma, and 2800–2600 Ma to have been derived from the extensively exposed metasedimentary rocks of the Yukon composite terrane located north of the Cantwell basin (Figure 1). Zircons of these ages have been well documented from primary and secondary sources across Laurentia (Table 1).

8. Regional Paleogeography of Mid- to Late Cretaceous Foreland Basin Depositional Systems: Next Steps

We interpret the Cantwell basin to have formed in a proximal part of a now-dismembered, regionally extensive Cretaceous foreland basin system that was bordered to the south by an active magmatic arc system (Figure 12). During the deposition of the Cantwell Formation,

defining components of the southern Alaska convergent margin located south of the paired foreland basin and arc system included marine and terrestrial depositional systems of the Matanuska forearc basin and the Chugach accretionary complex (Figure 12) [83,128–132]. Inboard of the magmatic arc, Mid–Late Cretaceous foreland basin depositional systems underwent a general transition from marine to non-marine depositional environments. The proximal terrestrial depocenters appear to have been spatially isolated and concentrated near the hinterland and magmatic arc (Figure 12). These depocenters include the Beaver Lake formation in the eastern Alaska Range (mid-Cretaceous) [126], the Caribou Pass formation in the northern Talkeetna Mountains (mid-Cretaceous) [103], and possibly the Panorama Peak formation in the central Alaska Range (Upper Cretaceous) [133]. It is important to recognize that all Cretaceous terrestrial strata located south of the Denali fault system have been displaced along the fault away from their original depositional location.

　　An important unresolved issue is the stratigraphic and temporal connections between the Cantwell Formation and other Cretaceous foreland basin strata that cover a large part of interior Alaska. Eight to twelve kilometers of Cretaceous strata of the Kuskokwim Group are exposed in central and southwestern Alaska [134–136]. Most of the marine strata of the Kuskokwim Group range in age from Albian to Campanian [134]. A tuff in the Kuskokwim Group with an age of 77 Ma reported by Miller and Bundtzen [137], however, makes the upper part of this section temporally equivalent with the deposition of the Cantwell Formation. Roughly 200 km north of the Cantwell basin are exposures of the poorly dated and highly deformed Jurassic–Cretaceous strata of the Manley basin e.g., Refs. [138,139]. Northeast of the Cantwell basin, extensive Cretaceous strata of the Kandik basin have been incorporated into the Charley River thrust belt [140,141]. We tentatively interpret the Kuskokwim, Manley, and Kandik basins to represent more distal, largely marine parts of the Cretaceous foreland basin system that were connected to the Cantwell basin by the Maastrichtian but have subsequently been dismembered by Cenozoic strike-slip faults and regional shortening e.g., Refs. [110,135,136].

　　Future studies are required to better define the nature of the sedimentary relationships between the Cantwell basin and other Cretaceous strata in the interior of Alaska. Results of these studies will be important for refining the regional extent and paleogeographic configuration of the Cretaceous foreland basin system and interior seaways. Further integration of sedimentological and paleontological data from southern, interior, and northern Alaska should result in an improved understanding of high-latitude ecosystems and the evolution of their vertebrate fauna. To resolve these connections between northern and southern Alaska would represent a significant step forward in addressing questions such as how temperature and precipitation trends over the represented range of paleo-latitudes impacted the evolution and seasonal or longer-term migration of large-bodied herbivore populations e.g., Ref. [7]. Ultimately, the integration of Cretaceous high-latitude depositional systems, paleo flora and fauna, and paleoclimate in Alaska has the potential to bear on paleogeographic connections between northwestern North America and Eurasia, but much more work is needed.

9. Conclusions

(1)　A thorough geologic and paleogeographic characterization of the Cantwell Formation is important because it provides a stratigraphic framework for recent and future paleontological and paleoclimate investigations of a Late Cretaceous high-latitude ecosystem. Our stratigraphic data allow the Cantwell Formation to be divided into two mappable members. The lower member, the Polychrome member (minimum thickness: ~1500 m), consists of wet alluvial fan, braided stream, and coastal fluvial strata. The upper member, the Cabin Creek–Double Mountain member (minimum thickness: ~1200 m), was deposited in estuarine and coastal lacustrine depositional environments. The coastal fluvial and tidal environments are associated with the remarkable preservation of vertebrate trackways such as theropods, hadrosaurs, and wading birds.

(2)　The configuration of the Cantwell basin was heavily influenced by syndepositional deformation along the northern and southern basin margins. In our study area, the basin margins are defined by opposing thrust belts, including a previously undocumented south-verging thrust system along the northern basin margin. The Cantwell Formation was deformed within these basinward propagating thrust systems from the Late Cretaceous through the Paleocene. Upper Paleocene–lower Eocene volcanic strata of the Teklanika formation were deposited unconformably atop the Cantwell Formation, and contractional deformation of both formations continued through at least the early Eocene.

(3)　U-Pb detrital zircon data from the Cantwell Formation (n = 4657) indicate that sediment was sourced from a coeval Late Cretaceous magmatic arc, as well as older exhumed Cretaceous plutonic sources. Plutons of the Late Cretaceous arc system that bordered the southern margin of the basin during the deposition of the Cantwell Formation are now exposed ~400 km to the southwest in the western Alaska Range due to dextral offset along the Denali fault system. Sediment sources north of the Cantwell basin included Upper Triassic–Lower Jurassic plutonic rocks of the Taylor Mountain batholith, as well as metamorphic rocks of the ancestral North American margin that provided recycled Proterozoic and Archean detrital zircons. Other secondary (recycled sedimentary) sources of sediment include Paleozoic and Mesozoic metasedimentary strata exposed in syndepositional thrust sheets along the margins of the basin and the Upper Jurassic–Cretaceous Kahiltna assemblage.

(4)　The Cantwell basin is interpreted to have formed in the proximal part of a now-dismembered foreland basin system and drained to the northeast into a Late Cretaceous interior seaway. Future studies may seek to better define the stratigraphic relationships between the interior seaway, likely represented by relatively unstudied Cretaceous strata of interior Alaska, and terrestrial and estuarine depositional systems of south-central and northern Alaska. These regional datasets would serve to better integrate disparate records of the Cretaceous high-latitude paleo-landscape of Alaska and would contribute to our understanding of relationships between depositional systems, faunal populations, and basinal settings. These datasets may also be critical for understanding paleogeographic and faunal connections between northwestern North American and Eurasia.

References

1. Hickman, R.G.; Sherwood, K.W.; Craddock, C. Structural Evolution of the Early Tertiary Cantwell Basin, South Central Alaska. *Tectonics* **1990**, *9*, 1433–1449. [CrossRef]
2. Ridgway, K.D.; Trop, J.M.; Sweet, A.R. Thrust-Top Basin Formation along a Suture Zone, Cantwell Basin, Alaska Range: Implications for Development of the Denali Fault System. *Geol. Soc. Am. Bull.* **1997**, *109*, 505–523. [CrossRef]
3. Tomsich, C.S.; McCarthy, P.J.; Fiorillo, A.R.; Stone, D.B.; Benowitz, J.A.; O'Sullivan, P.B. New Zircon U-Pb Ages for the Lower Cantwell Formation: Implications for the Late Cretaceous Paleoecology and Paleoenvironment of the Lower Cantwell Formation near Sable Mountain, Denali National Park and Preserve, Central Alaska Range, USA. In Proceedings of the International Conference on Arctic Margins VI, Fairbanks, AK, USA, May 30–June 2 2011; VSEGEI: St. Petersburg, Russia, 2014; pp. 19–60.
4. Fiorillo, A.R.; Hasiotis, S.T.; Kobayashi, Y.; Breithaupt, B.H.; McCarthy, P.J. Bird Tracks from the Upper Cretaceous Cantwell Formation of Denali National Park, Alaska, USA: A New Perspective on Ancient Northern Polar Vertebrate Biodiversity. *J. Syst. Palaeontol.* **2011**, *9*, 33–49. [CrossRef]
5. Fiorillo, A.R.; McCarthy, P.J.; Flaig, P.P. A Multi-Disciplinary Perspective on Habitat Preferences among Dinosaurs in a Cretaceous Arctic Greenhouse World, North Slope, Alaska (Prince Creek Formation: Lower Maastrichtian). *Palaeogeogr. Palaeoclimatol. Palaeoecol.* **2016**, *441*, 377–389. [CrossRef]
6. Fiorillo, A.R.; McCarthy, P.J.; Kobayashi, Y.; Tomsich, C.S.; Tykoski, R.S.; Lee, Y.; Tanaka, T.; Noto, C.R. An Unusual Association of Hadrosaur and Therizinosaur Tracks within Late Cretaceous Rocks of Denali National Park, Alaska. *Sci. Rep.* **2018**, *8*, 12. [CrossRef]
7. Fiorillo, A.R.; McCarthy, P.J.; Kobayashi, Y.; Suarez, M.B. Cretaceous Dinosaurs across Alaska Show the Role of Paleoclimate in Structuring Ancient Large-Herbivore Populations. *Geosciences* **2022**, *12*, 161. [CrossRef]
8. Salazar-Jaramillo, S. Paleoclimate and Paleoenvironment of the Prince Creek and Cantwell Formations, Alaska: Terrestrial Evidence of a Middle Maastrichtian Greenhouse Event. Master's Thesis, University of Alaska, Fairbanks, AK, USA, 2014.
9. Tomsich, C.S.; McCarthy, P.J.; Fowell, S.J.; Sunderlin, D. Paleofloristic and Paleoenvironmental Information from a Late Cretaceous (Maastrichtian) Flora of the Lower Cantwell Formation near Sable Mountain, Denali National Park, Alaska. *Palaeogeogr. Palaeoclimatol. Palaeoecol.* **2010**, *295*, 389–408. [CrossRef]
10. Cole, R.B.; Ridgway, K.D.; Layer, P.W.; Drake, J. Kinematics of Basin Development during the Transition from Terrane Accretion to Strike-Slip Tectonics. Late Cretaceous-Early Tertiary Cantwell Formation, South Central Alaska. *Tectonics* **1999**, *18*, 1224–1244. [CrossRef]
11. Trop, J.M.; Benowitz, J.A.; Cole, R.B.; O'Sullivan, P. Cretaceous to Miocene Magmatism, Sedimentation, and Exhumation within the Alaska Range Suture Zone: A Polyphase Reactivated Terrane Boundary. *Geosphere* **2019**, *15*, 1066–1101. [CrossRef]
12. Druckenmiller, M.L.; Moon, T.A.; Thoman, R.L.; Ballinger, T.J.; Berner, L.T.; Bernhard, G.H.; Bhatt, U.S.; Bjerke, J.W.; Box, J.E.; Brown, R.; et al. The Arctic. *Bull. Am. Meteorol. Soc.* **2021**, *102*, S263–S316. [CrossRef]
13. Thoman, R.L.; Richter-Menge, J.; Druckenmiller, M.L. *Arctic Report Card 2020 Executive Summary*; Arctic Report Card; NOAA: Washington, DC, USA, 2020; pp. 1–4.
14. Fiorillo, A.R.; Hasiotis, S.T.; Kobayashi, Y.; Tomsich, C.S. A Pterosaur Manus Track from Denali National Park, Alaska, Range, Alaska, United States. *PALAIOS* **2009**, *24*, 466–472. [CrossRef]
15. Fiorillo, A.R.; Hasiotis, S.T.; Kobayashi, Y. Herd Structure in Late Cretaceous Polar Dinosaurs: A Remarkable New Dinosaur Tracksite, Denali National Park, Alaska, USA. *Geology* **2014**, *42*, 719–722. [CrossRef]
16. Fiorillo, A.R.; Contessi, M.; Kobayashi, Y.; Mccarthy, P.J. Theropod Tracks from the Lower Cantwell Formation (Upper Cretaceous) of Denali National Park, Alaska, USA with Comments on Theropod Diversity in an Ancient, High-Latitude Terrestrial Ecosystem. In *Fossil Footprints of Western North America*; Lockley, M.G., Lucas, S.G., Eds.; NMMNHS Bulletin; New Mexico Museum of Natural History and Science: Albuquerque, NM, USA, 2014; pp. 429–449.
17. Fiorillo, A.R.; Adams, T.L. A Therizinosaur Track from the Lower Cantwell Formation (Upper Cretaceous) of Denali National Park, Alaska. *PALAIOS* **2012**, *27*, 395–400. [CrossRef]
18. Stewart, D.G. Vertebrate Ichnology and Paleoenvironmental Associations of Alaska's Largest Dinosaur Track Site in the Cretaceous Cantwell Formation (Maastrichtian) of Denali National Park and Preserve. Master's Thesis, University of Alaska Fairbanks, Fairbanks, AK, USA, 2020.
19. Pasch, A.D.; May, K.C. *First Occurrence of a Hadrosaur (Dinosauria) from the Matanuska Formation (Turonian) in the Talkeetna Mountains of South-Central Alaska*; Alaska Division of Geological & Geophysical Surveys: Fairbanks, AK, USA, 1998; pp. 99–109.

20. Fiorillo, A.R.; Kobayashi, Y.; McCarthy, P.J.; Tanaka, T.; Tykoski, R.S.; Lee, Y.-N.; Takasaki, R.; Yoshida, J. Dinosaur Ichnology and Sedimentology of the Chignik Formation (Upper Cretaceous), Aniakchak National Monument, Southwestern Alaska; Further Insights on Habitat Preferences of High-Latitude Hadrosaurs. *PLoS ONE* **2019**, *14*, e0223471. [CrossRef]

21. Fiorillo, A.R.; Adams, T.L.; Kobayashi, Y. New Sedimentological, Palaeobotanical, and Dinosaur Ichnological Data on the Palaeoecology of an Unnamed Late Cretaceous Rock Unit in Wrangell-St. Elias National Park and Preserve, Alaska, USA. *Cretac. Res.* **2012**, *37*, 291–299. [CrossRef]

22. Fiorillo, A.R.; Fanti, F.; Hults, C.; Hasiotis, S.T. New Ichnological, Paleobotanical, and Detrital Zircon Data from an Unnamed Rock Unit in Yukon-Charley Rivers National Preserve (Cretaceous: Alaska): Stratigraphic Implications for the Region. *PALAIOS* **2014**, *29*, 16–26. [CrossRef]

23. Fiorillo, A.R.; McCarthy, P.J.; Flaig, P.P. Taphonomic and Sedimentologic Interpretations of the Dinosaur-Bearing Upper Cretaceous Strata of the Prince Creek Formation, Northern Alaska: Insights from an Ancient High-Latitude Terrestrial Ecosystem. *Palaeogeogr. Palaeoclimatol. Palaeoecol.* **2010**, *295*, 376–388. [CrossRef]

24. Brown, C.M.; Druckenmiller, P. Basal Ornithopod (Dinosauria: Ornithischia) Teeth from the Prince Creek Formation (Early Maastrichtian) of Alaska. *Can. J. Earth Sci.* **2011**, *48*, 1342–1354. [CrossRef]

25. Mori, H.; Druckenmiller, P.; Erickson, G. A New Arctic Hadrosaurid (Dinosauria: Hadrosauridae) from the Prince Creek Formation (Lower Maastrichtian) of Northern Alaska. *Acta Palaeontol. Pol.* **2016**, *61*, 15–32. [CrossRef]

26. Spicer, R.A.; Herman, A.B. The Late Cretaceous Environment of the Arctic: A Quantitative Reassessment Based on Plant Fossils. *Palaeogeogr. Palaeoclimatol. Palaeoecol.* **2010**, *295*, 423–442. [CrossRef]

27. Flaig, P.P.; McCarthy, P.J.; Fiorillo, A.R. A Tidally Influenced, High-Latitude Coastal-Plain The Upper Cretaceous (Maastrichtian) Prince Creek Formation, North Slope, Alaska. In *From River to Rock Record: The Preservation of Fluvial Sediments and Their Subsequent Interpretation*; SEPM Special Publication; SEPM Society for Sedimentary Geology: Tulsa, OK, USA, 2011; pp. 233–264. ISBN 978-1-56576-305-0.

28. Chaney, R.W. Age of the Cantwell Formation. In *Proceedings of the Geological Society of America Proceedings 1936*; Geological Society of America: Boulder, CO, USA, 1937; pp. 355–356.

29. Imlay, R.W.; Reeside, J.B. Correlation of the Cretaceous Formations of Greenland and Alaska. *GSA Bull.* **1954**, *65*, 223–246. [CrossRef]

30. Wolfe, J.A.; Wahrhaftig, C. The Cantwell Formation of the Central Alaska Range. In *Changes in Stratigraphic Nomenclature by the U.S. Geological Survey, 1968*; U.S. Geological Survey Bulletin; United States Geological Survey: Denver, CO, USA, 1970; Volume 1294-A, pp. A41–A46.

31. Hickman, R.G. Structural Geology and Stratigraphy along a Segment of the Denali Fault System, Central Alaska Range, Alaska. Ph.D. Thesis, University of Wisconsin, Madison, WI, USA, 1974.

32. Sherwood, K.W. Stratigraphy, Metamorphic Geology, and Structural Geology of the Central Alaska Range, Alaska. Ph.D. Thesis, University of Wisconsin, Madison, WI, USA, 1979.

33. Csejtey, B.; Mullen, M.W.; Cox, D.P.; Gilbert, W.G.; Yeend, W.E.; Smith, T.E.; Wahrhaftig, C.; Craddock, C.; Brewer, W.M.; Sherwood, K.W.; et al. *Geology and Geochronology of the Healy Quadrangle, South-Central Alaska*; Open-File Report; United States Geological Survey: Denver, CO, USA, 1986; p. 92.

34. Csejtey, B.; Mullen, M.W.; Cox, D.P.; Stricker, G.D. *Geology and Geochronology of the Healy Quadrangle, South-Central Alaska*; United States Geological Survey: Denver, CO, USA, 1992; p. 63.

35. Reed, J.C. *Geology of the Mount McKinley Quadrangle, Alaska*; Mineral Resources of Alaska; United States Geological Survey: Denver, CO, USA, 1961; p. 43.

36. Gilbert, W.G.; Redman, E.C. *Geologic Map and Structure Sections of Healy C-6 Quadrangle, Alaska*; State of Alaska Department of Natural Resources Division of Geological and Geophysical Surveys; DGGS: Fairbanks, AK, USA, 1975; p. 3.

37. Jones, D.L.; Silberling, N.J.; Hillhouse, J. Wrangellia—A Displaced Terrane in Northwestern North America. *Can. J. Earth Sci.* **1977**, *14*, 2565–2577. [CrossRef]

38. Ridgway, K.D.; Trop, J.M.; Nokleberg, W.J.; Davidson, C.M.; Eastham, K.R. Mesozoic and Cenozoic Tectonics of the Eastern and Central Alaska Range: Progressive Basin Development and Deformation in a Suture Zone. *Geol. Soc. Am. Bull.* **2002**, *114*, 1480–1504. [CrossRef]

39. Brennan, P.R.K.; Gilbert, H.; Ridgway, K.D. Crustal Structure across the Central Alaska Range: Anatomy of a Mesozoic Collisional Zone: Crustal Structure of a Collisional Zone. *Geochem. Geophys. Geosyst.* **2011**, *12*, 1–23. [CrossRef]

40. Romero, M.C.; Ridgway, K.D.; Gehrels, G.E. Geology, U-Pb Geochronology, and Hf Isotope Geochemistry Across the Mesozoic Alaska Range Suture Zone (South-Central Alaska): Implications for Cordilleran Collisional Processes and Tectonic Growth of North America. *Tectonics* **2020**, *39*, 1–32. [CrossRef]

41. Waldien, T.S.; Roeske, S.M.; Benowitz, J.A. Tectonic Underplating and Dismemberment of the Maclaren-Kluane Schist Records Late Cretaceous Terrane Accretion Polarity and ~480 Km of Post-52 Ma Dextral Displacement on the Denali Fault. *Tectonics* **2021**, *40*, e2020TC006677. [CrossRef]

42. Hampton, B.A.; Ridgway, K.D.; Gehrels, G.E. A Detrital Record of Mesozoic Island Arc Accretion and Exhumation in the North American Cordillera: U-Pb Geochronology of the Kahiltna Basin, Southern Alaska: A Detrital Record of Arc Accretion. *Tectonics* **2010**, *29*, 1–21. [CrossRef]

43. Box, S.E.; Karl, S.M.; Jones, J.V.; Bradley, D.C.; Haeussler, P.J.; O'Sullivan, P.B. Detrital Zircon Geochronology along a Structural Transect across the Kahiltna Assemblage in the Western Alaska Range: Implications for Emplacement of the Alexander-Wrangellia-Peninsular Terrane against North America. *Geosphere* **2019**, *15*, 1774–1808. [CrossRef]

44. Trop, J.M.; Ridgway, K.D. Mesozoic and Cenozoic Tectonic Growth of Southern Alaska: A Sedimentary Basin Perspective. In *Tectonic Growth of a Collisional Continental Margin: Crustal Evolution of Southern Alaska*; Ridgway, K.D., Trop, J.M., Glen, J.M.G., O'Neill, J.M., Eds.; Geological Society of America Special Paper; Geological Society of America: Boulder, CO, USA, 2007; pp. 55–94. ISBN 978-0-8137-2431-7.

45. Keough, B.M.; Ridgway, K.D. Tectonic Growth of the Late Paleozoic-Middle Mesozoic Northwestern Margin of Laurentia and Implications for the Farewell Terrane: Stratigraphic, Structural, and Provenance Records from the Central Alaska Range. *Tectonics* **2021**, *40*, 1–35. [CrossRef]

46. Gilbert, W.G.; Ferrell, V.M.; Turner, D.L. *The Teklanika Formation—A New Paleocene Volcanic Formation in the Central Alaska Range*; Alaska Division of Geological & Geophysical Surveys: Fairbanks, AK, USA, 1976; p. 16.

47. Trop, J.M. Sedimentological, Provenance, and Structural Analysis of the Lower Cantwell Formation, Cantwell Basin, Central Alaska Range, Implications for the Development of a Thrust-Top Basin. Master's Thesis, Purdue University, West Lafayette, IN, USA, 1996.

48. Wilson, F.H.; Hults, C.P.; Mull, C.G.; Karl, S.M. *Geologic Map of Alaska*; U.S. Geological Survey Scientific Investigations Map 3340; United States Geological Survey: Anchorage, AK, USA, 2015.

49. Gehrels, G. Detrital Zircon U-Pb Geochronology: Current Methods and New Opportunities. In *Tectonics of Sedimentary Basins*; Busby, C., Azor, A., Eds.; John Wiley & Sons, Ltd.: Chichester, UK, 2012; pp. 45–62. ISBN 978-1-4443-4716-6.

50. Gehrels, G. Detrital Zircon U-Pb Geochronology Applied to Tectonics. *Annu. Rev. Earth Planet. Sci.* **2014**, *42*, 127–149. [CrossRef]

51. Gehrels, G.E.; Valencia, V.A.; Ruiz, J. Enhanced Precision, Accuracy, Efficiency, and Spatial Resolution of U-Pb Ages by Laser Ablation-Multicollector-Inductively Coupled Plasma-Mass Spectrometry: Technical Brief. *Geochem. Geophys. Geosyst.* **2008**, *9*, 1–13. [CrossRef]

52. Gehrels, G.; Pecha, M. Detrital Zircon U-Pb Geochronology and Hf Isotope Geochemistry of Paleozoic and Triassic Passive Margin Strata of Western North America. *Geosphere* **2014**, *10*, 49–65. [CrossRef]

53. Sundell, K.E.; Gehrels, G.E.; Pecha, M.E. Rapid U-Pb Geochronology by Laser Ablation Multi-Collector ICP-MS. *Geostand. Geoanalytical Res.* **2021**, *45*, 37–57. [CrossRef]

54. Stacey, J.S.; Kramers, J.D. Approximation of Terrestrial Lead Isotope Evolution by a Two-Stage Model. *Earth Planet. Sci. Lett.* **1975**, *26*, 207–221. [CrossRef]

55. Ludwig, K. *User's Manual for Isoplot Version 3.75–4.15: A Geochronological Toolkit for Microsoft Excel*; Special publication; Berkeley Geochronology Center: Berkeley, CA, USA, 2008.

56. Geisler, T.; Pidgeon, R.T.; van Bronswijk, W.; Kurtz, R. Transport of Uranium, Thorium, and Lead in Metamict Zircon under Low-Temperature Hydrothermal Conditions. *Chem. Geol.* **2002**, *191*, 141–154. [CrossRef]

57. Jo, H.R.; Rhee, C.W.; Chough, S.K. Distinctive Characteristics of a Streamflow-Dominated Alluvial Fan Deposit: Sanghori Area, Kyongsang Basin (Early Cretaceous), Southeastern Korea. *Sediment. Geol.* **1997**, *110*, 51–79. [CrossRef]

58. Ghinassi, M.; Ielpi, A. Morphodynamics and Facies Architecture of Streamflow-Dominated, Sand-Rich Alluvial Fans, Pleistocene Upper Valdarno Basin, Italy. In *Geology and Geomorphology of Alluvial and Fluvial Fans: Terrestrial and Planetary Perspectives*; Ventra, D., Clarke, L.E., Eds.; Geological Society of London: London, UK, 2018; Volume 440, pp. 175–200. ISBN 978-1-78620-267-3.

59. Ballance, P.F. Sheet-Flow-Dominated Gravel Fans of the Non-Marine Middle Cenozoic Simmler Formation, Central California. *Sediment. Geol.* **1984**, *38*, 337–359. [CrossRef]

60. Bull, W.B. Recognition of Alluvial Fan Deposits in the Stratigraphic Record. In *Recognition of Ancient Sedimentary Environments*; Rigby, J.K., Hamblin, W.K., Eds.; Society of Economic Paleontologists and Mineralogists Special Publication; SEPM Society for Sedimentary Geology: Tulsa, OK, USA, 1972; Volume 16, pp. 63–83.

61. Ridgway, K.D.; Decelles, P.G. Stream-Dominated Alluvial Fan and Lacustrine Depositional Systems in Cenozoic Strike-Slip Basins, Denali Fault System, Yukon Territory, Canada. *Sedimentology* **1993**, *40*, 645–666. [CrossRef]

62. Major, J.J. Depositional Processes in Large-Scale Debris-Flow Experiments. *J. Geol.* **1997**, *105*, 345–366. [CrossRef]

63. Collinson, J.D. Alluvial Sediments. In *Sedimentary Environments and Facies*; Reading, H.G., Ed.; Blackwell: Oxford, UK, 1986; pp. 20–62.

64. Smith, N.D.; Cross, T.A.; Dufficy, J.P.; Clough, S.R. Anatomy of an Avulsion. *Sedimentology* **1989**, *36*, 1–23. [CrossRef]

65. Cherven, V.B. Fluvial and Deltaic Facies in the Sentinel Butte Formation, Central Williston Basin. *SEPM JSR* **1978**, *48*, 159–170. [CrossRef]

66. Dalrymple, R.W.; Choi, K. Morphologic and Facies Trends through the Fluvial–Marine Transition in Tide-Dominated Depositional Systems: A Schematic Framework for Environmental and Sequence-Stratigraphic Interpretation. *Earth-Sci. Rev.* **2007**, *81*, 135–174. [CrossRef]

67. Reineck, H.-F.; Wunderlich, F. Classification and Origin of Flaser and Lenticular Bedding. *Sedimentology* **1968**, *11*, 99–104. [CrossRef]

68. Dalrymple, R.W. Tidal Depositional Systems. In *Facies Models 4*; Geotext; Geological Association of Canada: St. John's, NL, Canada, 2010; pp. 201–232. ISBN 978-1-897095-50-8.

69. Mutti, E.; Rosell, J.; Allen, G.P.; Fonessu, F.; Sgavetti, M. The Eocene Baronia Tide Dominated Delta-Shelf System in the Ager Basin. In *Excursion Guidebook, 6th European Regional Meeting. International Association of Sedimentologists, Lleida, Spain*; Milla, M.D., Rosell, J., Eds.; International Association of Sedimentologists: Gent, Belgium, 1985; pp. 579–600.

70. Schieber, J. Microbial Mats in Terrigenous Clastics: The Challenge of Identification in the Rock Record. *PALAIOS* **1999**, *14*, 3–12. [CrossRef]

71. Bose, S.; Chafetz, H.S. Morphology and Distribution of Miss: A Comparison Between Modern Siliciclastic and Carbonate Settings. In *Microbial Mats in Siliciclastic Depositional Systems Through Time*; Noffke, N., Chafetz, H., Eds.; SEPM Special Publication; SEPM Society for Sedimentary Geology: Tulsa, OK, USA, 2012; Volume 101, pp. 3–14. ISBN 978-1-56576-283-1.

72. Noffke, N.; Awramik, S. Stromatolites and MISS—Differences between Relatives. *GSA Today* **2013**, *23*, 4–9. [CrossRef]

73. Schieber, J.; Bose, P.K.; Eriksson, P.G.; Banerjee, S.; Sarkar, S.; Alterman, W.; Catuneanu, O. *Atlas of Microbial Mat Features Preserved within the Siliciclastic Rock Record: Atlases in Geosciences*; Elsevier: Amsterdam, The Netherlands, 2007.

74. Renaut, R.W.; Gierlowski-Kordesch, E.H. Lakes. In *Facies Models 4*; Geotext; Geological Association of Canada: St. John's, NL, Canada, 2010; pp. 541–576. ISBN 978-1-897095-50-8.

75. Hancock, J.M.; Kauffman, E.G. The Great Transgressions of the Late Cretaceous. *J. Geol. Soc. Lond.* **1979**, *136*, 175–186. [CrossRef]

76. Hancock, J.M. Transatlantic Correlations in the Campanian-Maastrichtian Stages by Eustatic Changes of Sea-Level. *Geol. Soc. Lond. Spec. Publ.* **1993**, *70*, 241–256. [CrossRef]

77. Braman, D.R.; Sweet, A.R. Terrestrial Palynomorph Biostratigraphy of the Cypress Hills, Wood Mountain, and Turtle Mountain Areas (Upper Cretaceous-Paleocene) of Western Canada. *Can. J. Earth Sci.* **1999**, *36*, 725–741. [CrossRef]

78. Fiorillo, A.R.; McCarthy, P.J.; Breithaupt, B.H.; Brease, P.F. Dinosauria and Fossil Aves Footprints from the Lower Cantwell Formation (Latest Cretaceous), Denali National Park and Preserve. In Proceedings of the Central Alaska Park Science Symposium, Denali, AK, USA, 12–14 September 2006; Alaska Regional Office, National Park Service, U.S. Department of Interior: Denali National Park and Preserve, AK, USA, 2007; Volume 6, pp. 41–43.

79. Allen, J.R.L. Subfossil Mammalian Tracks (Flandrian) in the Severn Estuary, S.W. Britain: Mechanics of Formation, Preservation and Distribution. *Phil. Trans. R. Soc. Lond. B* **1997**, *352*, 481–518. [CrossRef]

80. Epard, J.L.; Groshong, R.H. Kinematic Model of Detachment Folding Including Limb Rotation, Fixed Hinges and Layer-Parallel Strain. *Tectonophysics* **1995**, *247*, 85–103. [CrossRef]

81. Trop, J.M.; Ridgway, K.D. Petrofacies and Provenance of a Late Cretaceous Suture Zone Thrust-Top Basin, Cantwell Basin, Central Alaska Range. *J. Sediment. Res.* **1997**, *67*, 469–485. [CrossRef]

82. Christie-Blick, N.; Biddle, K.T. Deformation and Basin Formation along Strike-Slip Faults. In *Strike-Slip Deformation, Basin Formation, and Sedimentation*; Biddle, K.T., Christie-Blick, N., Eds.; SEPM Society for Sedimentary Geology: Tulsa, OK, USA, 1985; Volume 37, pp. 1–34. ISBN 978-1-56576-167-4.

83. Jones, J.V.; Todd, E.; Box, S.E.; Haeussler, P.J.; Holm-Denoma, C.S.; Karl, S.M.; Graham, G.E.; Bradley, D.C.; Kylander-Clark, A.R.C.; Friedman, R.M.; et al. Cretaceous to Oligocene Magmatic and Tectonic Evolution of the Western Alaska Range: Insights from U-Pb and 40Ar/39Ar Geochronology. *Geosphere* **2021**, *17*, 118–153. [CrossRef]

84. Koeneman, L.L.; Wilson, F.H. *Legacy K/Ar and 40Ar/39Ar Geochronologic Data from the Alaska-Aleutian Range Batholith of South-Central Alaska*; United States Geological Survey: Denver, CO, USA, 2018; p. 8.

85. Moll-Stalcup, E.J. Latest Cretaceous and Cenozoic Magmatism in Mainland Alaska. In *The Geology of Alaska*; Plafker, G., Berg, H.C., Eds.; Geological Society of America: Boulder, CO, USA, 1994; Volume G-1, ISBN 978-0-8137-5453-6.

86. Reed, B.L.; Lanphere, M.A. *Generalized Geologic Map of the Alaska-Aleutian Range Batholith Showing Potassium-Argon Ages of the Plutonic Rocks*; United States Geological Survey: Denver, CO, USA, 1972; 2 sheets.

87. Reed, B.L.; Lanphere, M.A. Alaska-Aleutian Range Batholith: Geochronology, Chemistry, and Relation to Circum-Pacific Plutonism. *Geol. Soc. Am. Bull.* **1973**, *84*, 2583–2610. [CrossRef]

88. Lanphere, M.A.; Reed, B.L. The McKinley Sequence of Granitic Rocks: A Key Element in the Accretionary History of Southern Alaska. *J. Geophys. Res.* **1985**, *90*, 11413–11430. [CrossRef]

89. Wallace, W.K.; Engebretson, D.C. Relationships between Plate Motions and Late Cretaceous to Paleogene Magmatism in Southwestern Alaska. *Tectonics* **1984**, *3*, 295–315. [CrossRef]

90. Wilson, F.H.; Smith, J.G.; Shew, N. Review of Radiometric Data from the Yukon Crystalline Terrane, Alaska and Yukon Territory. *Can. J. Earth Sci.* **1985**, *22*, 525–537. [CrossRef]

91. Day, W.C.; O'Neill, J.M.; Dusel-Bacon, C.; Aleinikoff, J.N.; Siron, C.R. *Geologic Map of the Kechumstuk Fault Zone in the Mount Veta Area, Fortymile Mining District, East-Central Alaska*; United States Geological Survey: Denver, CO, USA, 2014.

92. Dusel-Bacon, C.; Williams, I.S. Evidence for Prolonged Mid-Paleozoic Plutonism and Ages of Crustal Sources in East-Central Alaska from SHRIMP U–Pb Dating of Syn-Magmatic, Inherited, and Detrital Zircon. *Can. J. Earth Sci.* **2009**, *46*, 21–39. [CrossRef]

93. Aleinikoff, J.N. Geochronology of Augen Gneiss and Related Rocks, Yukon-Tanana Terrane, East-Central Alaska. *Geol. Soc. Am. Bull.* **1986**, *97*, 626–637. [CrossRef]

94. Day, W.C.; Aleinikoff, J.N.; Roberts, P.; Smith, M.; Gamble, B.M.; Henning, M.W.; Gough, L.P.; Morath, L.C. *Geologic Map of the Big Delta B-2 Quadrangle, East-Central Alaska*; United States Geological Survey: Denver, CO, USA, 2003.

95. Dusel-Bacon, C.; Aleinikoff, J.N. Petrology and Tectonic Significance of Augen Gneiss from a Belt of Mississippian Granitoids in the Yukon-Tanana Terrane, East-Central Alaska. *Geol. Soc. Am. Bull.* **1985**, *96*, 411–425. [CrossRef]

96. Dusel-Bacon, C.; Hopkins, M.J.; Mortensen, J.K.; Dashevsky, S.S.; Bressler, J.R.; Day, W.C. Paleozoic Tectonic and Metallogenic Evolution of the Pericratonic Rocks of East-Central Alaska and Adjacent Yukon. In *Paleozoic Evolution and Metallogeny of Pericratonic Terranes at the Ancient Pacific Marign of North America, Canadian and Alaskan Cordillera*; Colpron, M., Nelson, J.L., Eds.; Geological Association of Canada Special Papers; Geological Association of Canada: St. John's, NL, Canada, 2006; Volume 45, pp. 25–74.

97. Dusel-Bacon, C.; Wooden, J.L.; Hopkins, M.J. U-Pb Zircon and Geochemical Evidence for Bimodal Mid-Paleozoic Magmatism and Syngenetic Base-Metal Mineralization in the Yukon-Tanana Terrane, Alaska. *Geol. Soc. Am. Bull.* **2004**, *116*, 989–1015. [CrossRef]

98. Johnston, S.T.; Mortensen, J.K.; Erdmer, P. Igneous and Metaigneous Age Constraints for the Aishihik Metamorphic Suite, Southwest Yukon. *Can. J. Earth Sci.* **1996**, *33*, 1543–1555. [CrossRef]

99. Mortensen, J.K. Geology and U–Pb Geochronology of the Klondike District, West-Central Yukon Territory. *Can. J. Earth Sci.* **1990**, *27*, 903–914. [CrossRef]

100. Nelson, J.L.; Colpron, M.; Piercey, S.J.; Dusel-Bacon, C.; Murphy, D.C. Paleozoic Tectonic and Metallogenetic Evolution of Pericratonic Terranes in Yukon, Northern British Columbia and Eastern Alaska. In *Paleozoic Evolution and Metallogeny of Pericratonic Terranes at the Ancient Pacific Margin of North America, Canadian and Alaskan Cordillera*; Colpron, M., Nelson, J.L., Eds.; Geological Association of Canada Special Papers; Geological Association of Canada: St. John's, NL, Canada, 2006; Volume 45, pp. 323–360.

101. Greig, C.J.; Gehrels, G.E. U–Pb Zircon Geochronology of Lower Jurassic and Paleozoic Stikinian Strata and Tertiary Intrusions, Northwestern British Columbia. *Can. J. Earth Sci.* **1995**, *32*, 1155–1171. [CrossRef]

102. Kalbas, J.L.; Ridgway, K.D.; Gehrels, G.E. Stratigraphy, Depositional Systems, and Provenance of the Lower Cretaceous Kahiltna Assemblage, Western Alaska Range: Basin Development in Response to Oblique Collision. In *Tectonic Growth of a Collisional Continental Margin: Crustal Evolution of Southern Alaska*; Ridgway, K.D., Trop, J.M., Glen, J.M.G., O'Neill, J.M., Eds.; Geological Society of America Special Paper; Geological Society of America: Boulder, CO, USA, 2007; pp. 307–343. ISBN 978-0-8137-2431-7.

103. Hampton, B.A.; Ridgway, K.D.; O'Neill, J.M.; Gehrels, G.E.; Schmidt, J.; Blodgett, R.B. Pre-, Syn-, and Postcollisional Stratigraphic Framework and Provenance of Upper Triassic–Upper Cretaceous Strata in the Northwestern Talkeetna Mountains, Alaska. In *Tectonic Growth of a Collisional Continental Margin: Crustal Evolution of Southern Alaska*; Ridgway, K.D., Trop, J.M., Glen, J.M.G., O'Neill, J.M., Eds.; Geological Society of America Special Paper; Geological Society of America: Boulder, CO, USA, 2007; pp. 401–438. ISBN 978-0-8137-2431-7.

104. Hults, C.P.; Wilson, F.H.; Donelick, R.A.; O'Sullivan, P.B. Two Flysch Belts Having Distinctly Different Provenance Suggest No Stratigraphic Link between the Wrangellia Composite Terrane and the Paleo-Alaskan Margin. *Lithosphere* **2013**, *5*, 575–594. [CrossRef]

105. Pálfy, J.; Smith, P.L.; Mortensen, J.K.; Friedman, R.M. Integrated Ammonite Biochronology and U-Pb Geochronometry from a Basal Jurassic Section in Alaska. *Geol. Soc. Am. Bull.* **1999**, *111*, 1537–1549. [CrossRef]

106. Amato, J.M.; Rioux, M.E.; Kelemen, P.B.; Gehrels, G.E.; Clift, P.D.; Pavlis, T.L.; Draut, A.E. U-Pb Geochronology of Volcanic Rocks from the Jurassic Talkeetna Formation and Detrital Zircons from Prearc and Postarc Sequences: Implications for the Age of Magmatism and Inheritance in the Talkeetna Arc. In *Tectonic Growth of a Collisional Continental Margin: Crustal Evolution of Southern Alaska*; Ridgway, K.D., Trop, J.M., Glen, J.M.G., O'Neill, J.M., Eds.; Geological Society of America Special Paper; Geological Society of America: Boulder, CO, USA, 2007; pp. 253–271. ISBN 978-0-8137-2431-7.

107. Rioux, M.; Hacker, B.; Mattinson, J.; Kelemen, P.; Blusztajn, J.; Gehrels, G. Magmatic Development of an Intra-Oceanic Arc: High-Precision U-Pb Zircon and Whole-Rock Isotopic Analyses from the Accreted Talkeetna Arc, South-Central Alaska. *Geol. Soc. Am. Bull.* **2007**, *119*, 1168–1184. [CrossRef]

108. Rioux, M.; Mattinson, J.; Hacker, B.; Grove, M. Growth and Evolution of the Accreted Talkeetna Arc, South-Central Alaska: Solutions to the "Arc Paradox". In *Proceedings of the AGU Fall Meeting Abstracts*; American Geophysical Union: Washington DC, USA, 2002; p. V12C-11.

109. Rioux, M.; Mattinson, J.; Hacker, B.; Kelemen, P.; Blusztajn, J.; Hanghøj, K.; Gehrels, G. Intermediate to Felsic Middle Crust in the Accreted Talkeetna Arc, the Alaska Peninsula and Kodiak Island, Alaska: An Analogue for Low-Velocity Middle Crust in Modern Arcs: Talkeetna Arc Middle Crust. *Tectonics* **2010**, *29*, 1–17. [CrossRef]

110. Nokleberg, W.J.; Plafker, G.; Wilson, F.H.; Berg, H.C. Geology of South-Central Alaska. In *The Geology of Alaska*; Geological Society of America: Boulder, CO, USA, 1994; Volume G-1, pp. 311–366.

111. Plafker, G.; Nokleberg, W.J.; Lull, J.S. Bedrock Geology and Tectonic Evolution of the Wrangellia, Peninsular, and Chugach Terranes along the Trans- Alaska Crustal Transect in the Chugach Mountains and Southern Copper River Basin, Alaska. *J. Geophys. Res.* **1989**, *94*, 4255–4295. [CrossRef]

112. Roeske, S.M.; Snee, L.W.; Pavlis, T.L. Dextral-Slip Reactivation of an Arc-Forearc Boundary during Late Cretaceous-Early Eocene Oblique Convergence in the Northern Cordillera. In *Geology of a Transpressional Orogen Developed during Ridge-Trench Interaction along the North Pacific Margin*; Sisson, V.B., Roeske, S.M., Pavlis, T.L., Eds.; Geological Society of America Special Paper; Geological Society of America: Boulder, CO, USA, 2003; pp. 141–169. ISBN 978-0-8137-2371-6.

113. Day, E.M.; Pavlis, T.L.; Amato, J.M. Detrital Zircon Ages Indicate an Early Cretaceous Episode of Blueschist-Facies Metamorphism in Southern Alaska: Implications for the Mesozoic Paleogeography of the Northern Cordillera. *Lithosphere* **2016**, *8*, 451–462. [CrossRef]

114. Beranek, L.P.; McClelland, W.C.; van Staal, C.R.; Israel, S.; Gordee, S.M. Late Jurassic Flare-up of the Coast Mountains Arc System, NW Canada, and Dynamic Linkages across the Northern Cordilleran Orogen: Flare-Up of the Coast Mountains Arc. *Tectonics* **2017**, *36*, 877–901. [CrossRef]

115. Snyder, D.C.; Hart, W.K. The White Mountain Granitoid Suite: Isotopic Constraints on Source Reservoirs for Cretaceous Magmatism within the Wrangellia Terrane. In *Tectonic Growth of a Collisional Continental Margin: Crustal Evolution of Southern Alaska*; Ridgway, K.D., Trop, J.M., Glen, J.M.G., O'Neill, J.M., Eds.; Geological Society of America Special Paper; Geological Society of America: Boulder, CO, USA, 2007; pp. 379–399. ISBN 978-0-8137-2431-7.

116. Graham, G.E.; Kelley, K.D.; Holm-Denoma, C.S.; Ayuso, R.A.; Kokaly, R.F.; Hoefen, T.M.; Selby, D. Geochronology of Early Cretaceous Porphyry Cu Deposits in Eastern Alaska. In Proceedings of the 35th International Geological Congress, Capetown, South Africa, 27 August–4 September 2016.

117. Dusel-Bacon, C.; Holm-Denoma, C.S.; Jones, J.V.; Aleinikoff, J.N.; Mortensen, J.K. Detrital Zircon Geochronology of Quartzose Metasedimentary Rocks from Parautochthonous North America, East-Central Alaska. *Lithosphere* **2017**, *9*, 927–952. [CrossRef]

118. Ross, G.M. Precambrian Basement in the Canadian Cordillera: An Introduction. *Can. J. Earth Sci.* **1991**, *28*, 1133–1139. [CrossRef]

119. Rainbird, R.; Cawood, P.; Gehrels, G. The Great Grenvillian Sedimentation Episode: Record of Supercontinent Rodinia's Assembly. In *Tectonics of Sedimentary Basins*; Busby, C., Azor, A., Eds.; Recent Advances; Blackwell Publishing Ltd.: Chichester, UK, 2012; pp. 583–601. ISBN 978-1-4443-4716-6.

120. Brennan, P.R.K.; Ridgway, K.D. Detrital Zircon Record of Neogene Exhumation of the Central Alaska Range: A Far-Field Upper Plate Response to Flat-Slab Subduction. *Geol. Soc. Am. Bull.* **2015**, *127*, 945–961. [CrossRef]

121. Lease, R.O.; Haeussler, P.J.; O'Sullivan, P. Changing Exhumation Patterns during Cenozoic Growth and Glaciation of the Alaska Range: Insights from Detrital Thermochronology and Geochronology: Alaska Range Exhumation Patterns. *Tectonics* **2016**, *35*, 934–955. [CrossRef]

122. Eisbacher, G.H. Sedimentology of the Dezadeash Flysch and Its Implications for Strike-Slip Faulting along the Denali Fault, Yukon Territory and Alaska. *Can. J. Earth Sci.* **1976**, *13*, 1495–1513. [CrossRef]

123. Nokleberg, W.J.; Jones, D.L.; Silberling, N.J. Origin and Tectonic Evolution of the Maclaren and Wrangellia Terranes, Eastern Alaska Range, Alaska. *GSA Bull.* **1985**, *96*, 1251–1270. [CrossRef]

124. Fasulo, C.R.; Ridgway, K.D.; Trop, J.M. Detrital Zircon Geochronology and Hf Isotope Geochemistry of Mesozoic Sedimentary Basins in South-Central Alaska: Insights into Regional Sediment Transport, Basin Development, and Tectonics along the NW Cordilleran Margin. *Geosphere* **2020**, *16*, 1125–1152. [CrossRef]

125. Nokleberg, W.J.; Aleinikoff, J.N.; Dutro, J.T.; Lanphere, M.A.; Silberling, N.J.; Silva, S.R.; Smith, T.E.; Turner, D.L. *Map, Tables, and Summary of Fossil and Isotopic Age Data, Mount Hayes Quadrangle, Eastern Alaska Range, Alaska*; United States Geological Survey: Denver, CO, USA, 1992.

126. Trop, J.M.; Benowitz, J.A.; Koepp, D.Q.; Sunderlin, D.; Brueseke, M.E.; Layer, P.W.; Fitzgerald, P.G. Stitch in the Ditch: Nutzotin Mountains (Alaska) Fluvial Strata and a Dike Record ca. 117–114 Ma Accretion of Wrangellia with Western North America and Initiation of the Totschunda Fault. *Geosphere* **2020**, *16*, 29. [CrossRef]

127. Till, A.B.; Harris, A.G.; Wardlaw, B.R.; Mullen, M. Upper Triassic Continental Margin Strata of the Central Alaska Range: Implications for Paleogeographic Reconstruction. In *Tectonic Growth of a Collisional Continental Margin: Crustal Evolution of Southern Alaska*; Ridgway, K.D., Trop, J.M., Glen, J.M.G., O'Neill, J.M., Eds.; Geological Society of America Special Paper; Geological Society of America: Boulder, CO, USA, 2007; pp. 191–205. ISBN 978-0-8137-2431-7.

128. Trop, J.M.; Ravn, R.L. Sedimentology, Palynology, and Petrology of the Cretaceous Matanuska Formation, South-Central Alaska: Relationships between Forearc Basin Development and Accretionary Tectonic Events. In *Geological Society of America Abstracts with Programs*; Geological Society of America: Boulder, CO, USA, 2003; Volume 35, p. 559.

129. Trop, J.M. Latest Cretaceous Forearc Basin Development along an Accretionary Convergent Margin: South-Central Alaska. *Geol. Soc. Am. Bull.* **2008**, *120*, 207–224. [CrossRef]

130. Amato, J.M.; Pavlis, T.L. Detrital Zircon Ages from the Chugach Terrane, Southern Alaska, Reveal Multiple Episodes of Accretion and Erosion in a Subduction Complex. *Geology* **2010**, *38*, 459–462. [CrossRef]

131. Amato, J.M.; Pavlis, T.L.; Clift, P.D.; Kochelek, E.J.; Hecker, J.P.; Worthman, C.M.; Day, E.M. Architecture of the Chugach Accretionary Complex as Revealed by Detrital Zircon Ages and Lithologic Variations: Evidence for Mesozoic Subduction Erosion in South-Central Alaska. *Geol. Soc. Am. Bull.* **2013**, *125*, 1891–1911. [CrossRef]

132. Stevens Goddard, A.L.; Trop, J.M.; Ridgway, K.D. Detrital Zircon Record of a Mesozoic Collisional Forearc Basin in South Central Alaska: The Tectonic Transition from an Oceanic to Continental Arc. *Tectonics* **2018**, *37*, 529–557. [CrossRef]

133. Huff, C.J. Paleozoic to Neogene Stratigraphic and Structural History of the Alaska Range Suture Zone, North of the Denali Fault, East Central Alaska Range. Master's Thesis, University of California Davis, Davis, CA, USA, 2012.

134. Box, S.E.; Elder, W.P. Depositional and Biostratigraphic Framework of the Upper Cretaceous Kuskokwim Group, Southwestern Alaska. In *Geologic Studies in Alaska by the U.S. Geological Survey, 1990*; Bradley, D.C., Ford, A.B., Eds.; U.S. Geological Survey Bulletin 1999; U.S. Geological Survey: Denver, CO, USA, 1992; pp. 8–16.

135. Decker, J.; Bergman, S.C.; Blodgett, R.B.; Box, S.E.; Bundtzen, T.K.; Clough, J.G.; Coonrad, W.L.; Gilbert, W.G.; Miller, M.L.; Murphy, J.M.; et al. Geology of Southwestern Alaska. In *The Geology of Alaska*; Plafker, G., Berg, H.C., Eds.; The Geology of North America; Geological Society of America: Boulder, CO, USA, 1994; Volume G-1, pp. 285–310. ISBN 978-0-8137-5219-8.

136. Miller, M.L.; Bradley, D.C.; Bundtzen, T.K.; McClelland, W. Late Cretaceous through Cenozoic Strike-Slip Tectonics of Southwestern Alaska. *J. Geol.* **2002**, *110*, 247–270. [CrossRef]

137. Miller, M.L.; Bundtzen, T.K. *Generalized Geologic Map of the Iditarod Quadrangle, Alaska, Showing Potassium-Argon, Major-Oxide, Trace-Element, Fossil, Paleocurrent, and Archaeological Sample Localities*; United States Geological Survey: Reston, VA, USA, 1994; p. 48.

138. Weber, F.R.; Wheeler, K.L.; Rinehart, C.D.; Chapman, R.M.; Blodgett, R.B. *Geologic Map of the Livengood Quadrangle, Alaska*; United States Geological Survey: Denver, CO, USA, 1992; p. 20.

139. Weber, F.R.; Wheeler, K.L.; Rinehart, C.D.; Light, T.D. *Generalized Geologic Map of the Livengood Quadrangle, Alaska*; United States Geological Survey: Denver, CO, USA, 1997; 20p, 1 sheet.

140. Dover, J.H. Geology of Part of East-Central Alaska. In *The Geology of Alaska*; Plafker, G., Berg, H.C., Eds.; Geological Society of America: Boulder, CO, USA, 1994; Volume G-1, pp. 135–155. ISBN 978-0-8137-5453-6.

141. Johnsson, M.J. Tectonic Assembly of East-Central Alaska: Evidence from Cretaceous–Tertiary Sandstones of the Kandik River Terrane. *Geol. Soc. Am. Bull.* **2000**, *112*, 1023–1042. [CrossRef]